2019

REFINING THE ONSET TIMING AND SLIP HISTORY ALONG THE NORTHERN PART OF THE TETON FAULT

Rachel Montague Hoar
University of Kentucky, hoarrm@gmail.com
Digital Object Identifier: https://doi.org/10.13023/etd.2019.021

STUDENT AGREEMENT:

I represent that my thesis or dissertation and abstract are my original work. Proper attribution has been given to all outside sources. I understand that I am solely responsible for obtaining any needed copyright permissions. I have obtained needed written permission statement(s) from the owner(s) of each third-party copyrighted matter to be included in my work, allowing electronic distribution (if such use is not permitted by the fair use doctrine) which will be submitted to UKnowledge as Additional File.

I hereby grant to The University of Kentucky and its agents the irrevocable, non-exclusive, and royalty-free license to archive and make accessible my work in whole or in part in all forms of media, now or hereafter known. I agree that the document mentioned above may be made available immediately for worldwide access unless an embargo applies.

I retain all other ownership rights to the copyright of my work. I also retain the right to use in future works (such as articles or books) all or part of my work. I understand that I am free to register the copyright to my work.

REVIEW, APPROVAL AND ACCEPTANCE

The document mentioned above has been reviewed and accepted by the student's advisor, on behalf of the advisory committee, and by the Director of Graduate Studies (DGS), on behalf of the program; we verify that this is the final, approved version of the student's thesis including all changes required by the advisory committee. The undersigned agree to abide by the statements above.

Rachel Montague Hoar, Student

Dr. J. Ryan Thigpen, Major Professor

Dr. Ed Woolery, Director of Graduate Studies

REFINING THE ONSET TIMING AND SLIP HISTORY ALONG THE NORTHERN PART OF THE TETON FAULT

Thesis

A thesis submitted in partial fulfillment of the requirements for the degree of Master of Science in the College of Arts and Sciences at the University of Kentucky

By

Rachel Montague Hoar

Lexington, Kentucky

Director: Dr. J. Ryan Thigpen, Assistant Professor of Earth and Environmental Sciences

Lexington, Kentucky

2018

ABSTRACT OF THESIS

REFINING THE ONSET TIMING AND SLIP HISTORY
ALONG THE NORTHERN PART OF THE TETON FAULT

A new apatite (U-Th)/He (AHe) dataset from subvertical transects collected in the Teton and Gallatin Ranges in the Teton-Yellowstone region provides insight for the slip history and length of the Teton fault. Along the northernmost segment of the Teton fault, inverse thermal history modeling of AHe data from Eagles Rest Peak yield a ~9 Ma age for onset of fault slip. This age supports previous interpretations that Mount Moran may be the true center of the Teton fault. This refined interpretation coupled with length-displacement fault scaling analysis and previous estimates of total fault displacement (~6 km) indicates that the Teton fault may extend 50-90 km north of Mount Moran. However, this new data precludes the possibility that the Teton and East Gallatin faults represent the same structure. Yet, because these systems share a similar structure trend and initial slip ages (13 Ma and 16 Ma, respectively), they may still be related at a larger scale. To the south, the Teewinot transect yields the oldest onset age of ~32 Ma, however a >500 m vertical data gap in this transect leads us to cautiously interpret the results of this model, particularly as this age conflicts with four other transects along-strike.

KEY WORDS: Normal Faulting, Apatite (U-Th)/He Thermochronology, Inverse Thermal History Models, Fault Growth Scaling Relationships, Teton Fault, Yellowstone Hotspot

Rachel Montague Hoar

December 14, 2018

REFINING THE ONSET TIMING AND SLIP HISTORY ALONG THE NORTHERN PART OF THE TETON FAULT

By

Rachel Montague Hoar

Dr. J. Ryan Thigpen
Director of Thesis

Dr. Ed Woolery
Director of Graduate Studies

December 14, 2018

DEDICATION

To my loving parents, Melissa and John Hoar

ACKNOWLEDGEMENTS

Words cannot describe my many thanks to my M.S. advisor, Dr. Ryan Thigpen. Ryan, this thesis would have not been successful without your expert guidance, selfless time, and patience. Your motivation and dedication to your work is exactly what I was looking for in an advisor. It is infectious and brings out my inner tiger too. One of the best things about working for you was that I felt like you really understood me as person. You saw my drive and enthusiasm to become a better researcher/geologist and day in and day out worked with me to help strengthen my weak areas as well as build-up confidence in my stronger ones. I truly found the right mentor at the right time in my life. Thanks for being the best coach that I have ever had.

Summer Brown, I consider you one of my mentors as well because you essentially created this project that I get to stand on the shoulders of. I will forever be in-debt to you for paving the way for this research, as getting to work on this project is easily the most rewarding experience of my life to date. In addition, your professional guidance has helped me become more aware in general and prepared me to know what to expect in industry, and I am so very thankful for that.

I would also like to extend my gratitude to my committee members, Dr. Moecher and Dr. Guenthner. Dr. Moecher, your easygoingness made me more at ease and relaxed, especially when I just needed someone to be like, it's fine Rachel, just chill… and also because you let me call you Moech-Dogg!. Willy Guenthner, thank you so much for

working with me and helping me to analyze my samples. Your involvement in the methodology and analyses of this research work is extremely appreciated.

Next, I would like to thank my fellow graduate peers in my research lab (Stephanie, Meredith, Brandon), your support as friends and colleagues is something that I could only wish for in a research lab. Brandon, I don't think I could ever get sick of your dry humor, you are truly a treat. Meredith, I cannot thank you enough for helping me with both sample processing and sample analyses. I'll never forget that three-day trip (which felt like six-days) when we slaved over the He line to run almost all of my samples, you are the definition of a trooper. Stephanie, I am so happy we hit-it-off! Thank you for your countless hours of emotional support as well as being such a smarty too, I couldn't have made it to the finish-line without you on my side. In addition to the graduate students in my lab group, I would like to give a special shout-out to my favorite undergrad, Ryan Parks. Parks, you and I made quite the team. Thank you for helping me process *every single one* of my samples, you are amazing.

Outside of my research lab, I owe a big thanks our department in general, especially Adrianne, Dr. Woolery, and Pete; I do not know what I would have done without you all's constant support and help whenever I needed anything. In addition, I want to extend my thanks to others that helped me collect samples in the field including Paul Johnston, Bart Melton, and my personal favorite Rex Thigpen. Rex, it's obvious where Ryan gets his humor from, you two are a hoot!

Several close friends not only provided me with much needed TLC throughout my time at UKY, but also assisted me in this research, or did both! Bisrat Zelalem, you always had a way of getting me to see the bigger picture when I would get down at times overstressing the small stuff. Those reality checks kept me focused on the task at hand, thank you. Also, if it weren't for your wake-up phone calls to me, I would have overslept so many classes in the last four years (between JMU and UKY) that I probably wouldn't have made it here. Patrick Whalen, you've become one of my favorite people that I met along this journey. Also, I am very grateful for your help during that first field season. Aside from helping to carry some of my samples from the back country, that dingo-dango bit that you and Ryan would do was the only thing that distracted me from thinking about my screaming calves. Michael Suavman and Mitchell Clay, both of you are great friends and I really appreciate you all's savvy reviewing/editing skills when I just couldn't look at my writing any longer. Jonathan Wilson, your kindness and friendship has been really special to me, thank you. Also, your mastery of ArcGIS is exceptional and am so gracious to for spending hours and hours to help create some of the maps in this study.

Lastly but certainly not least, I would like to thank my family and friends at home, especially my Mom, Dad, and sister, Olivia. You all are my favorite people and I most definitely would not have gotten to where I am without your constant love and support of my aspirations and goals. I cannot describe how much it means to me to be a part of such a tight-knit and loving family. You all will always be my favorite rocks.

TABLE OF CONTENTS

LIST OF TABLES

LIST OF FIGURES

1. INTRODUCTION

The Teton fault, a crustal-scale normal fault in northwestern Wyoming, drives exhumation of the Teton Range in the footwall and subsidence of the Jackson Hole Valley in the hanging wall (Fig. 1.1). The modern fault scarp offsets Quaternary lateral moraine features along the range front (up to 27 m total offset; Grand Teton National Park, 2014) and even younger lake sediments visible in CHIRP seismic data in the northern part of Jackson Lake (Figs. 1.2 and 1.3; Thigpen et al., 2018). Additionally, trenching studies indicate multiple post-Pinedale glaciation (~13 ka) slip events with average offsets of ~2 m, including prehistoric ruptures of 2.8 m and 1.3 m at 7,900 and 4,800 yrs., respectively (White et al., 2009). Despite the evidence for recent Quaternary slip and the position of this structure within the most seismically active portion of the intermountain western U.S. (Smith and Arabasz, 1991; White et al., 2009), the Teton fault has not produced a major earthquake in recorded history, producing a persistent enigma in regard to the earthquake hazard potential of this structure. Multiple studies have proposed that a major slip event on the Teton fault has the potential to produce a M_w >7.0 earthquake (Byrd et al., 1994; White et al., 2009). However, key to model predictions is understanding the slip history and total length and linkage of the Teton fault system.

The timing of Teton fault initiation and subsequent range uplift has been interpreted by various stratigraphic (Barnosky, 1984; Roberts and Burbank, 1993; Love et al., 1997; Love et al., 2003), structural (Lageson, 1992; Lageson et al., 1999; Morgan and McIntosh, 2005; Leopold, 2007; Camp et al., 2015) and paleo seismic (Byrd et al.,

1994; Hampel et al., 2007) studies to range from 25 – 2 Ma and thus could either be related to Basin and Range uplift (Smith and Arabasz, 1991), more recent encroachment of the Yellowstone hotspot (~2 Ma; Anders et al., 1989; Anders and Sleep 1992; Pierce and Morgan, 2009), or some combination of both. In a recent study, Brown et al. (2017) utilized apatite U-Th/He (AHe) thermochronology of samples collected from subvertical transects in the Teton fault footwall along the length of the range to constrain the timing of rapid cooling of the footwall, which is interpreted to represent fault motion.

In the Brown et al. (2017) study, inverse thermal history modeling of the AHe data reveal that the oldest motion on the Teton fault initiated between 15-13 Ma in the vicinity of Mount Moran (Figs. 1.4a, 1.4d, and 1.5). This slip onset age led that study to suggest that motion along the Teton fault was related to Basin and Range extension. However, because the Brown et al. (2017) modeled time-temperature histories suggest that uplift continues along the Teton fault in the present-day, it is possible that more recent motion (<2 Ma) could be associated with migration of the Yellowstone hot-spot to its current position (Fig. 1.1a).

A second conclusion of the Brown et al. (2017) study is that slip onset ages and rates vary substantially along-strike. As mentioned previously, inverse thermal history modeling of AHe data from the Mount Moran transect (Fig. 1.4d) yields slip onset ages of 15-13 Ma. To the south, however, similar models of AHe data collected near the Grand Teton and Rendezvous Peak yield slip onset ages of ~10 Ma and ~7 Ma, respectively. By incorporating these data with traditional normal fault growth models wherein faults grow from the center out to the tips and thus yield the oldest ages at or near the fault center (Cowie and Scholz, 1992a; Dawers et al., 1993; Manighetti et al.,

2001; Kim and Sanderson, 2005), Brown et al. (2017) proposed that Mount Moran may represent the center of the Teton fault. This interpretation lies in stark contrast with traditional interpretations that the Grand Teton represents the approximate center of the fault (Love et al., 1997). If Mount Moran does indeed represent the center of the Teton fault, as proposed by Brown et al. (2017), that would imply that the Teton fault should continue much further north. Using minimum vertical throw estimates of ~6 km derived from combining AHe data with normal fault growth models and observed fault scaling relationships (Dawers et al., 1995; Manighetti et al., 2001; Densmore et al., 2004; Gudmumdsson, 2004; Densmore et al., 2005; Gudmundsson, 2013), Brown et al. (2017) further proposed that the Teton fault should extend 30-100 km farther north than previously realized (Fig. 1.6). In this scenario, Brown et al. (2017) explained that the absence of major observable footwall relief is due to migration of the Yellowstone hotspot to its present location (Fig. 1.1a) at ~2 Ma, which caused erasure of the northernmost extension of a paleo-Teton fault (Fig. 1.7)

Although this idea is certainly intriguing, additional work is required to further constrain the evolution of the Teton fault. First, the southernmost transect (Grand Teton and Rendezvous) collected by Brown et al. (2017) was composed of only three samples, as sedimentary rocks in that area lacked ideal apatite yield necessary for a comprehensive AHe study (Fig. 1.5b). Secondly, the Grand Teton transect was also composed of only three samples and the highest elevation sample was collected a lateral distance of ~2.5 km from the projected fault surface, possibly limiting its utility for constraining fault motion (Fig. 1.5c). Lastly, Mount Moran represents the most northern transect collected in the Brown et al. (2017) study, so we currently have no constraints for fault motion

north of that transect. To address these challenges, this study collected three new sample transects at Static Peak between the previous Rendezvous and Grand Teton transects, at Teewinot Mountain adjacent to the Grand transect but much closer to the projected Teton fault plane, and at Eagles Rest Peak to the north of Mount Moran. Of these three sample transects, two of them (Mt. Teewinot and Eagles Rest Peak) were analyzed for the study presented herein (Figs. 1.5d, 1.8b and 1.9). Additionally, this study collected a transect from the Gallatin Range north of Yellowstone, which represents the maximum northern extension of the Teton fault proposed by Brown et al. (2017) (Fig.1.6c, Fig. 1.8). Specifically, we use the data from the these new transects to answer the following questions: (1) Does Mt. Moran represent the true center of the Teton fault? If so, what implications does that have on our understanding of the growth development of this fault system and its potential to have once had a longer along-strike expression?; (2) If the Teton fault was initially longer than indicated by the present-day footwall topography preserved as the Teton Range, how much further north does it actually extend and is it possible that the East Gallatin fault along the front of the Gallatin Range may be a relict northern portion of the paleo-Teton fault?

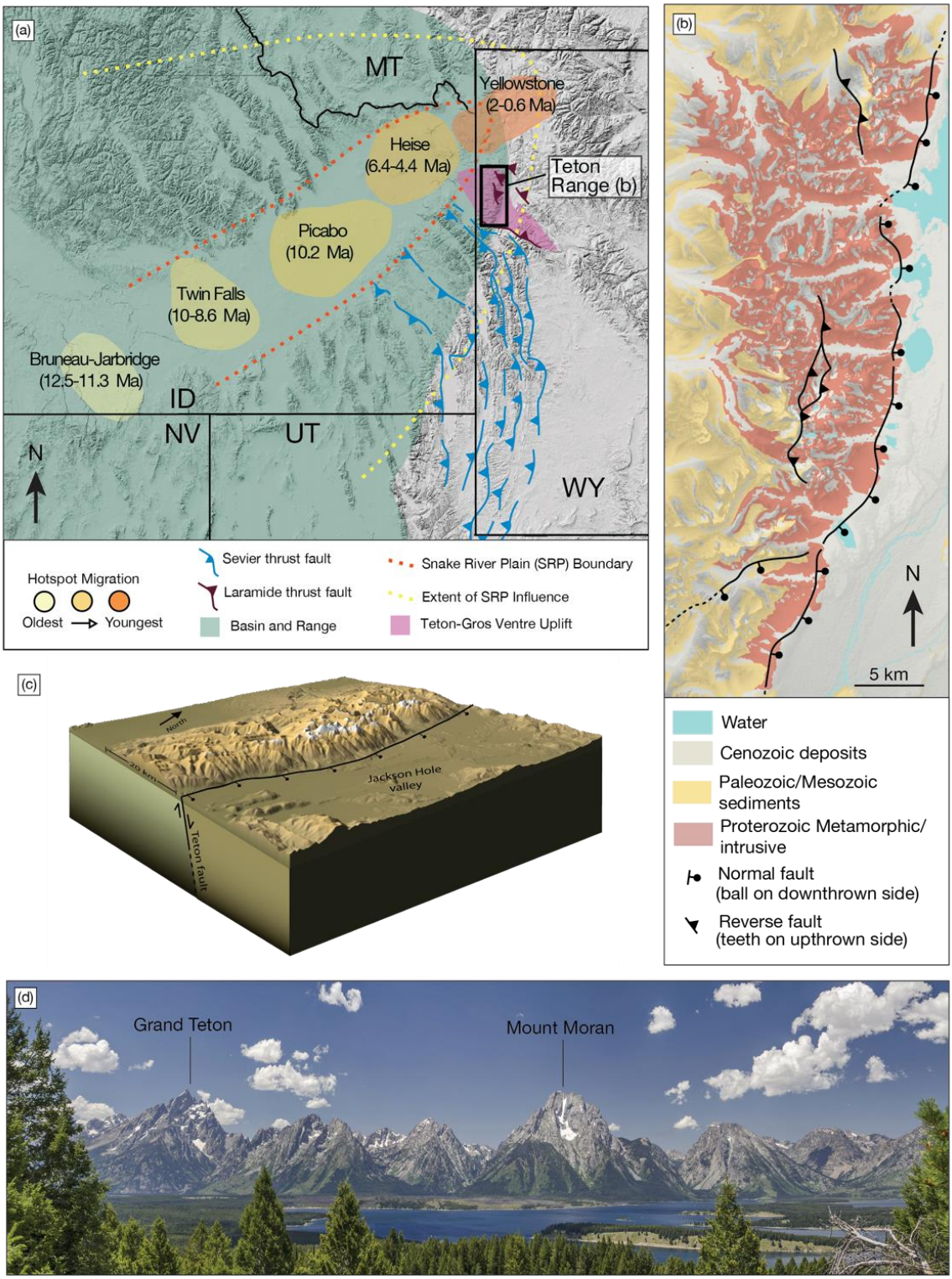
(a)
MT
Yellowstone
(2-0.6 Ma)
Heise
(6.4-4.4 Ma)
Teton
Range (b)
Picabo
(10.2 Ma)
Twin Falls
(10-8.6 Ma)
Bruneau-Jarbridge
(12.5-11.3 Ma)
ID
NV
UT
WY
N
Hotspot Migration
Oldest
Youngest
Sevier thrust fault
Laramide thrust fault
Basin and Range
Snake River Plain (SRP) Boundary
Extent of SRP Influence
Teton-Gros Ventre Uplift
(b)
N
5 km
Water
Cenozoic deposits
Paleozoic/Mesozoic sediments
Proterozoic Metamorphic/ intrusive
Normal fault (ball on downthrown side)
Reverse fault (teeth on upthrown side)
(c)
North
30 km
Jackson Hole valley
Teton fault
(d)
Grand Teton
Mount Moran

Figure 1.1. (a) Digital elevation map of the western-U.S. highlighting the overlapping regional geologic provinces (Sevier, Laramide, Basin and Range, present-day Yellowstone hotspot) that intersect at our study area in the Teton-Yellowstone region in northwestern Wyoming. (b) Regional geologic map of the Teton Range. (c) 3D block model of the Teton Range showing the N10E striking Teton normal fault and resulting uplift of the Teton range footwall to the west and subsidence of the Jackson Hole valley to the east. (d) View of the central and northern Teton Range from Signal Mountain overlook (facing west). After Brown et al. (2017).

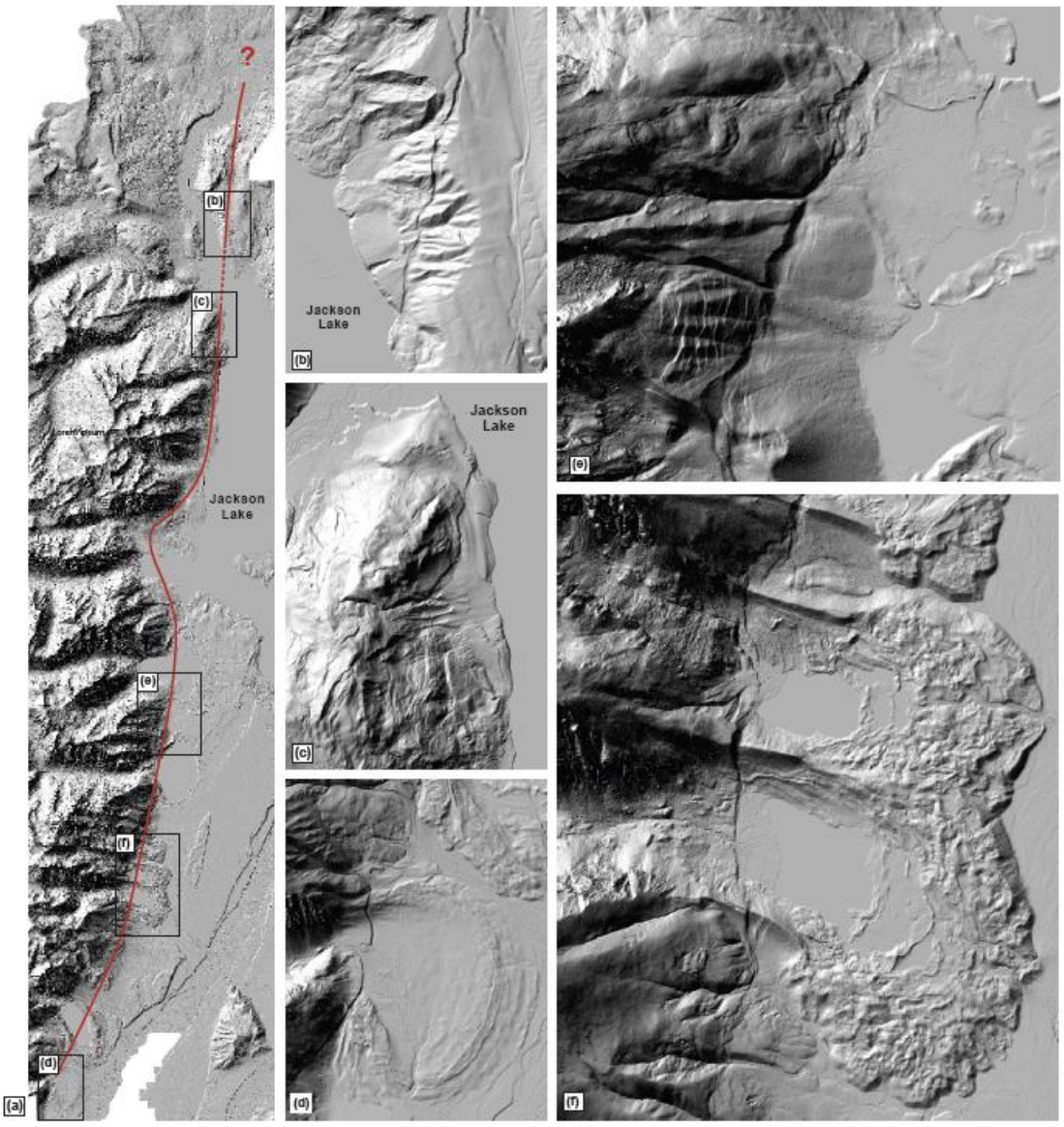

Figure 1.2. (a) LiDAR image (National Park Service, 2014) that shows the expression of the Teton fault in much detail along the Teton Range and further north. (b) and (c) show offset of approximately 12 m seen in the northernmost reaches of the fault suggesting that it extends northward beneath Jackson Lake, tracts back on land and potentially extends more to the north thereafter. (d), (e), and (f) show significant offset along Quaternary glacial moraines indicating the recent activity along this structure with offsets up to 27 m. After Thigpen et al. (2018).

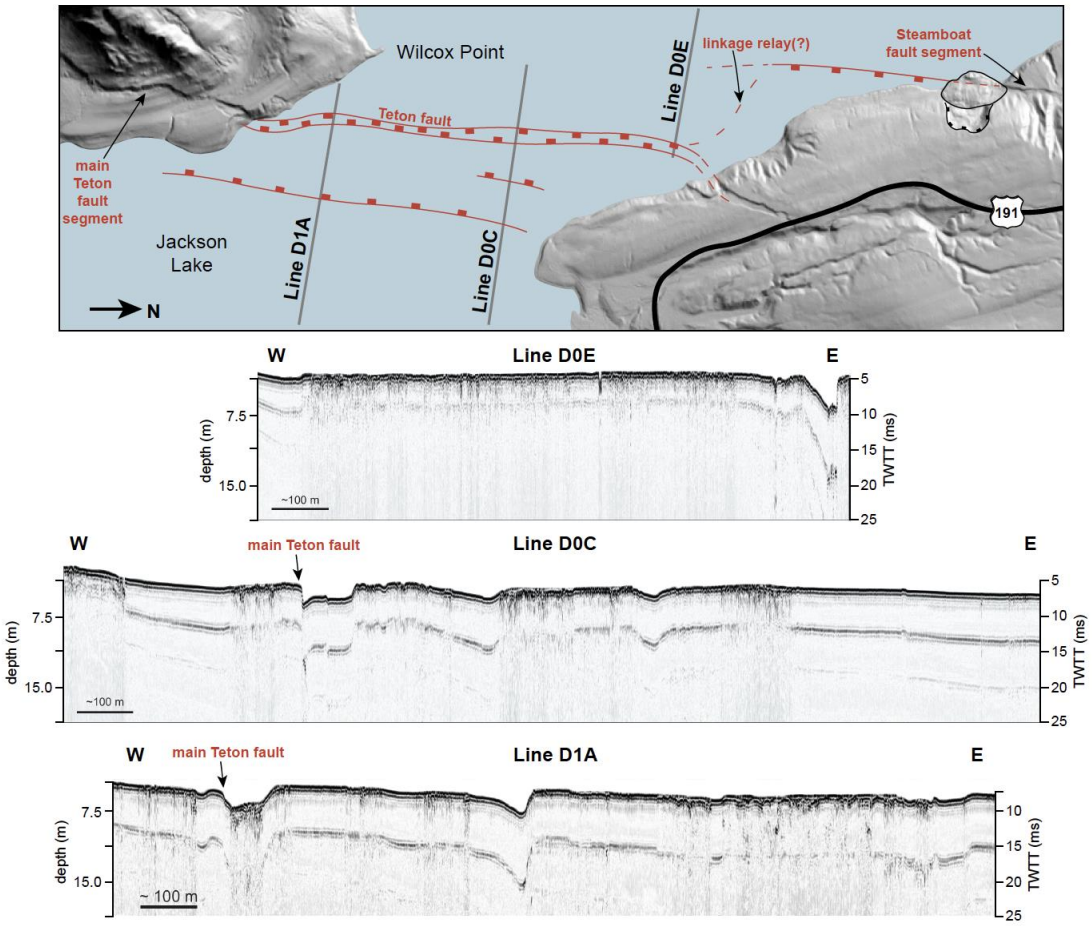

Figure 1.3. Figure showing evidence of antithetic fault segments mapped via CHIRP seismic in the northern part of Jackson Lake. These x-section lines running from W (near the main segment of the fault) to the east reveal very recent slip history and support our interpretation of a northern extent of the Teton fault. After Thigpen et al. (in prep).

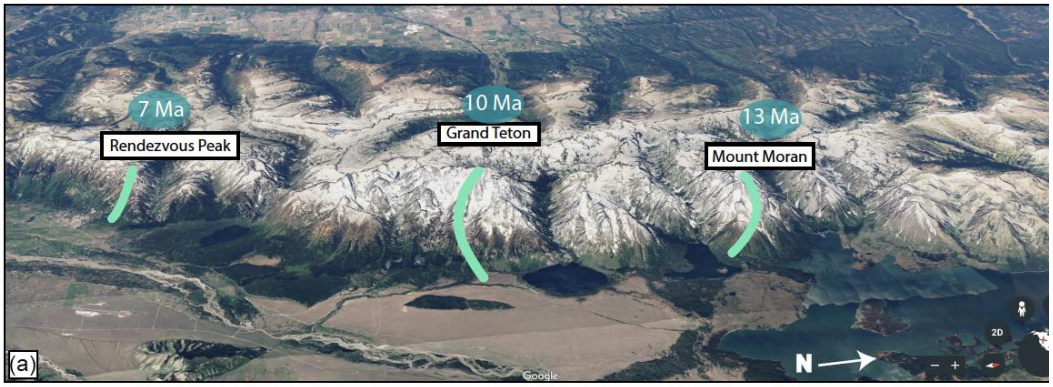
7 Ma
Rendezvous Peak
10 Ma
Grand Teton
13 Ma
Mount Moran
(a)
N

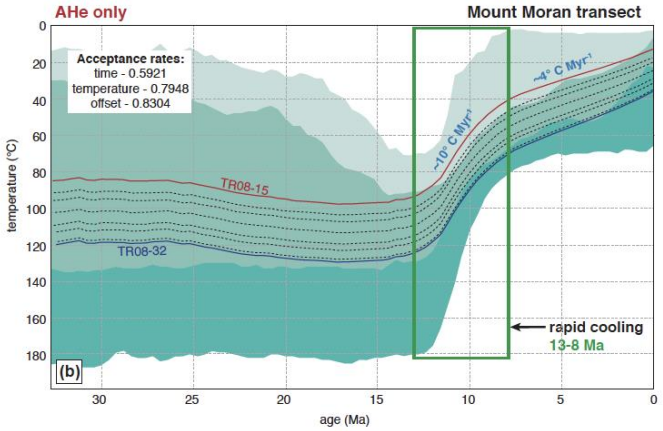
AHe only
Mount Moran transect
Acceptance rates:
time - 0.5921
temperature - 0.7948
offset - 0.8304
~4° C Myr⁻¹
~10° C Myr⁻¹
TR08-15
TR08-32
rapid cooling
13-8 Ma
(b)
temperature (°C)
age (Ma)

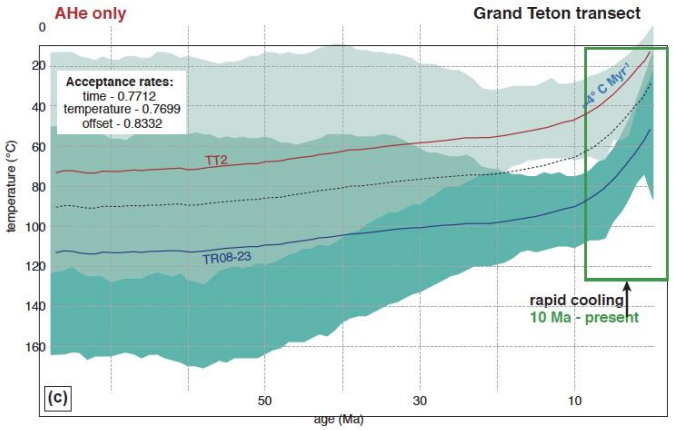
AHe only
Grand Teton transect
Acceptance rates:
time - 0.7712
temperature - 0.7699
offset - 0.8332
~4° C Myr⁻¹
TT2
TR08-23
rapid cooling
10 Ma - present
(c)
temperature (°C)
age (Ma)

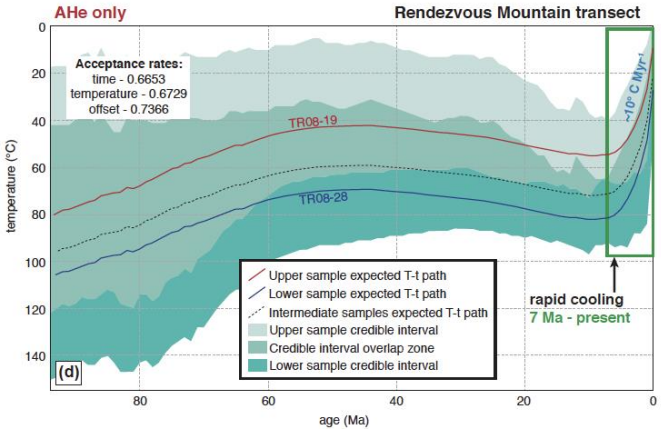
AHe only
Rendezvous Mountain transect
Acceptance rates:
time - 0.6653
temperature - 0.6729
offset - 0.7366
~10° C Myr⁻¹
TR08-19
TR08-28
Upper sample expected T-t path
Lower sample expected T-t path
Intermediate samples expected T-t path
Upper sample credible interval
Credible interval overlap zone
Lower sample credible interval
rapid cooling
7 Ma - present
(d)
temperature (°C)
age (Ma)

Figure 1.4: Summary of Brown et al. (2017) study. Figure 1.4a. shows locations along Teton Range for each AHe sample transect. From north to south these are: Mount Moran, with an onset age of 13 Ma; Grand Teton, with an onset age of 10 Ma; and Rendezvous Peak, with an onset age of 7Ma. Figures 1.4b (Moran), 1.4c (Grand Teton), 1.4d (Rendezvous) are the QTQt inverse thermal history models for each of the transects, respectively. In each model the green boxes are used to highlight the onset age of rapid exhumation in response to slip along the Teton fault. Collectively, these transect reveal a southward progression of slip onset along the Teton fault. After Brown et al., 2017 and Modified from Thigpen et al. (2018).

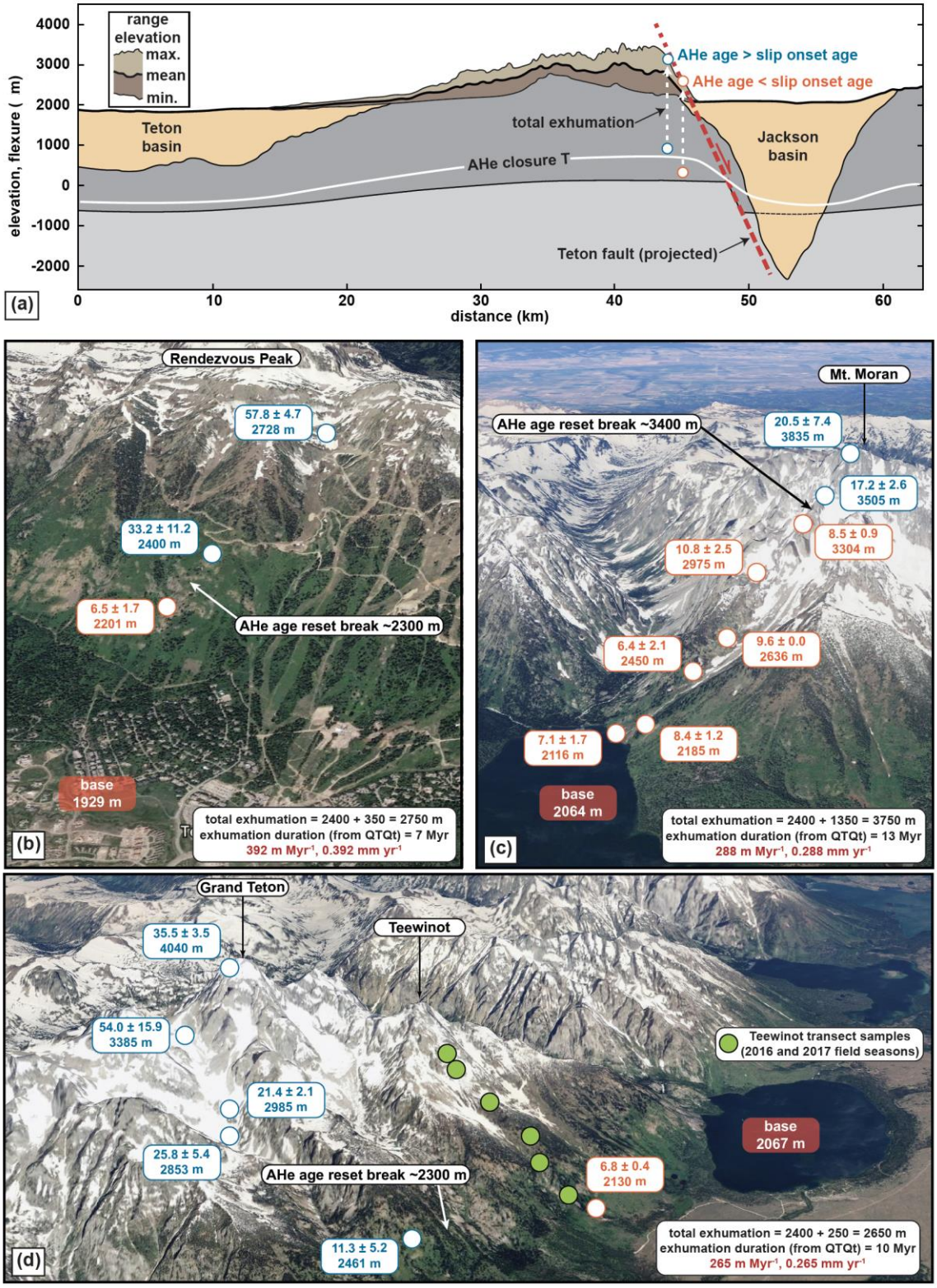
range elevation
max.
mean
min.
AHe age > slip onset age
AHe age < slip onset age
Teton basin
total exhumation
Jackson basin
AHe closure T
Teton fault (projected)
elevation, flexure (m)
distance (km)
(a)
Rendezvous Peak
57.8 ± 4.7
2728 m
33.2 ± 11.2
2400 m
6.5 ± 1.7
2201 m
AHe age reset break ~2300 m
base
1929 m
total exhumation = 2400 + 350 = 2750 m
exhumation duration (from QTQt) = 7 Myr
392 m Myr-1, 0.392 mm yr-1
(b)
Mt. Moran
AHe age reset break ~3400 m
20.5 ± 7.4
3835 m
17.2 ± 2.6
3505 m
8.5 ± 0.9
3304 m
10.8 ± 2.5
2975 m
6.4 ± 2.1
2450 m
9.6 ± 0.0
2636 m
7.1 ± 1.7
2116 m
8.4 ± 1.2
2185 m
base
2064 m
total exhumation = 2400 + 1350 = 3750 m
exhumation duration (from QTQt) = 13 Myr
288 m Myr-1, 0.288 mm yr-1
(c)
Grand Teton
Teewinot
35.5 ± 3.5
4040 m
54.0 ± 15.9
3385 m
21.4 ± 2.1
2985 m
25.8 ± 5.4
2853 m
AHe age reset break ~2300 m
11.3 ± 5.2
2461 m
Teewinot transect samples
(2016 and 2017 field seasons)
base
2067 m
6.8 ± 0.4
2130 m
total exhumation = 2400 + 250 = 2650 m
exhumation duration (from QTQt) = 10 Myr
265 m Myr-1, 0.265 mm yr-1
(d)

Figure 1.5. Onset of footwall uplift from subvertical sample transects. (a) Schematic diagram in cross-sectional view of the of the projected Teton normal fault (red dotted line) with the Teton Range in the (exhumed) footwall and the Jackson Hole valley in the (subsided) hanging wall. Circles represent the rock samples and their locations collected along the subvertical transect. It is assumed that each of these samples contains apatite to be dated with the apatite-He method. Blue circles indicate samples that, prior to Teton faulting, resided in the upper crust at lower temperatures than the apatite-He closer temperature, Tc (~70°C*). Red circles represent the samples that, prior to Teton faulting resided at higher temperatures than the apatite-He Tc. By collecting numerous samples in the footwall, we can identify the break between the blue samples and red samples along the transect. This break identifies the onset time (age) of rapid exhumation in response to Teton normal faulting. 1.5b, 1.5c, and 1.5d are Google Earth images of the relative sample locations from the Brown et al. (2017) subvertical transects with the colors of each circle aligning with those in the schematic cross-section diagram in 1.5a in order to determine the inflection point or onset age of footwall cooling along these transects. (b) Rendezvous Peak transect samples and corresponding AHe ages. (c) Mt. Moran transect samples and corresponding AHe ages. (d) Grand Teton transect samples and corresponding AHe age in comparison to the locations of samples collected along the new the Mt. Teewinot transect of this study, in order to represent that the new Teewinot transect was collected because it has a higher elevation gradient and is closer to the projected Teton fault plane than the Grand Teton transect samples. After Thigpen et al. (2018).*

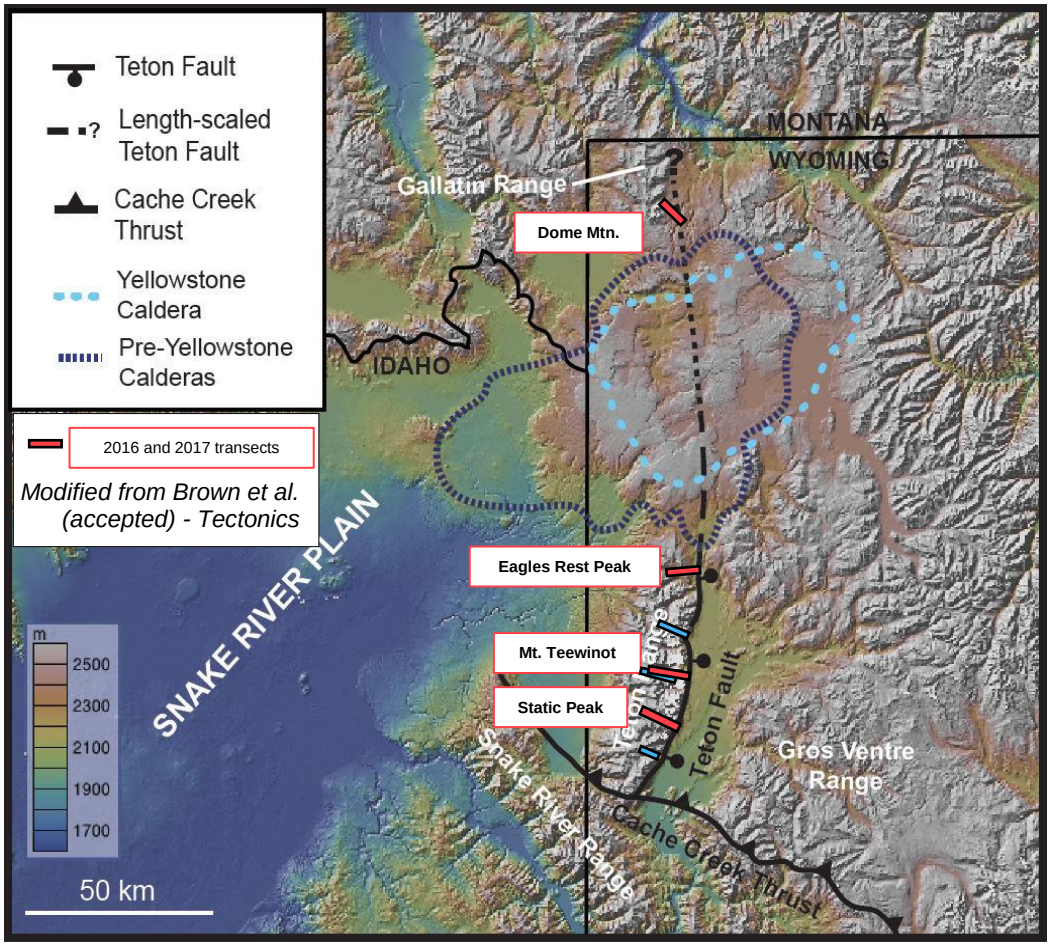

Figure 1.6. Shaded relief map of the hypothesized extent of the paleo-Teton fault from Brown et al., 2017 and sample transect locations within the study area. New sample transects in this study are indicated by red lines. Previous sample transects from the Brown et al. (2017) study are indicated by blue lines. The projected Teton fault length will be tested in this study from the new subvertical transect collected at the northernmost end of the Teton Range at Eagles Rest Peak Also, the new Dome Mountain transect collected at the southern end of the Gallatin Range was collected to analyze if the E-Gallatin fault slip history relates to the Teton fault in a way that would suggest whether these two normal faults, which have a similar structural trend were potentially once one large normal fault system prior to the migration of the Yellowstone hotspot into the area. Thus, this figure leads to the suggestion the Yellowstone hotspot encroachment into the region caused erasure of the northernmost extent of the Teton fault.

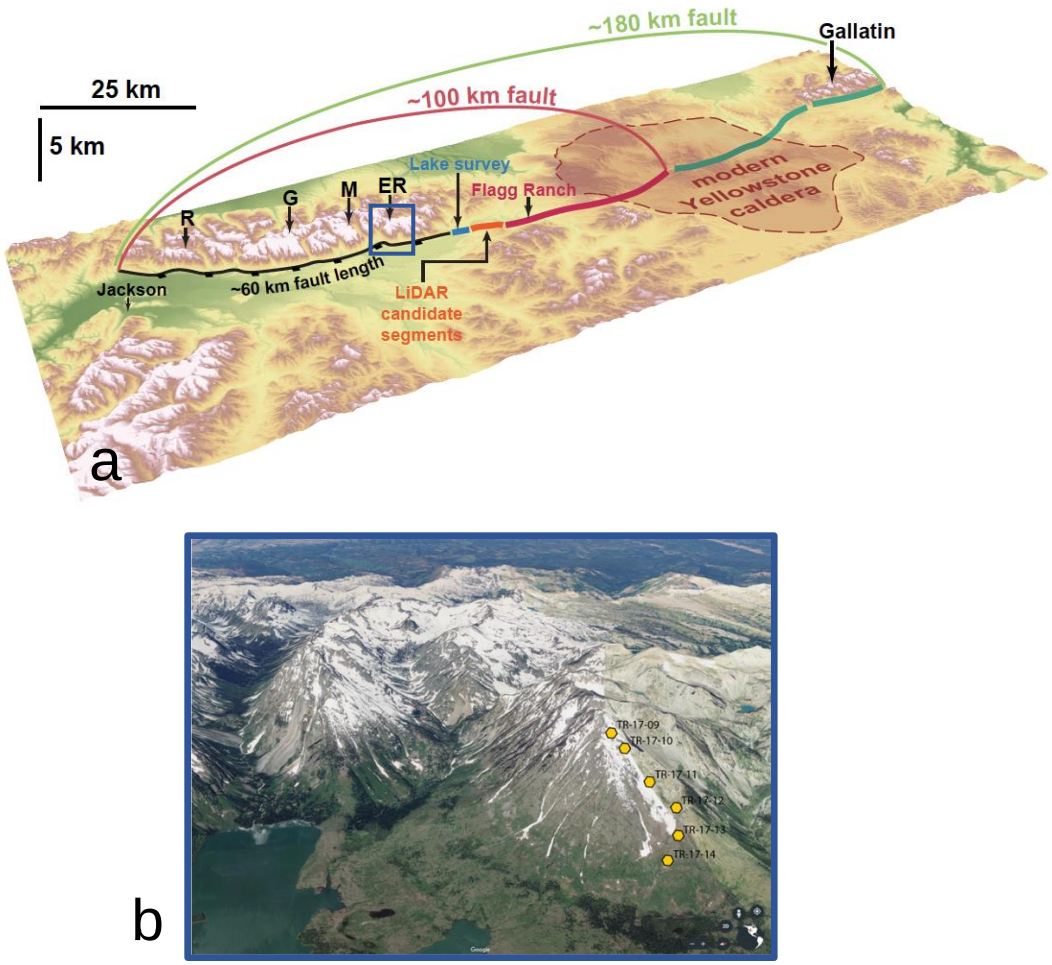

Figure 1.7. Schematic Teton fault projection and Eagles Rest transect (a) Similar to Fig. 1.6 but looking at the Teton fault facing NW and showing projected length of the Teton fault to north along strike based on the minimum estimate of D_{max} of 6 km found from AHe ages collected along the Mt. Moran transect. Based on L:D_{max} scaling for normal faults, we assume that if onset ages are seen to get older further north of Mt. Moran (i.e. if they are older at Eagles Rest Peak) then a D_{max} of 6 km should scale to length of the Teton fault between 100-180 km, putting the original extent as far north as the Gallatin Range. Similarly, if ages are seen to get younger north of Mt. Moran, then this would support that near Mt. Moran is the location where the Teton fault first initiated. Nevertheless, if Mt. Moran is the center, the Teton fault would still project north of its present-day mapped length, but not far enough into the Gallatin Range. Thus, samples collected from the Gallatin Range and Eagles Rest Peak transects will address both where the center of the Teton fault and in relation its original along-strike length. Support for northward extension of the fault is also seen from lake seismic and LiDAR imaging (Thigpen et al., 2018 and Thigpen et al., in press). (b) Google Earth image of the locations for samples collected along the Eagles Rest Peak transect, corresponding to blue box in (a). Modified from Thigpen et al. (2018).

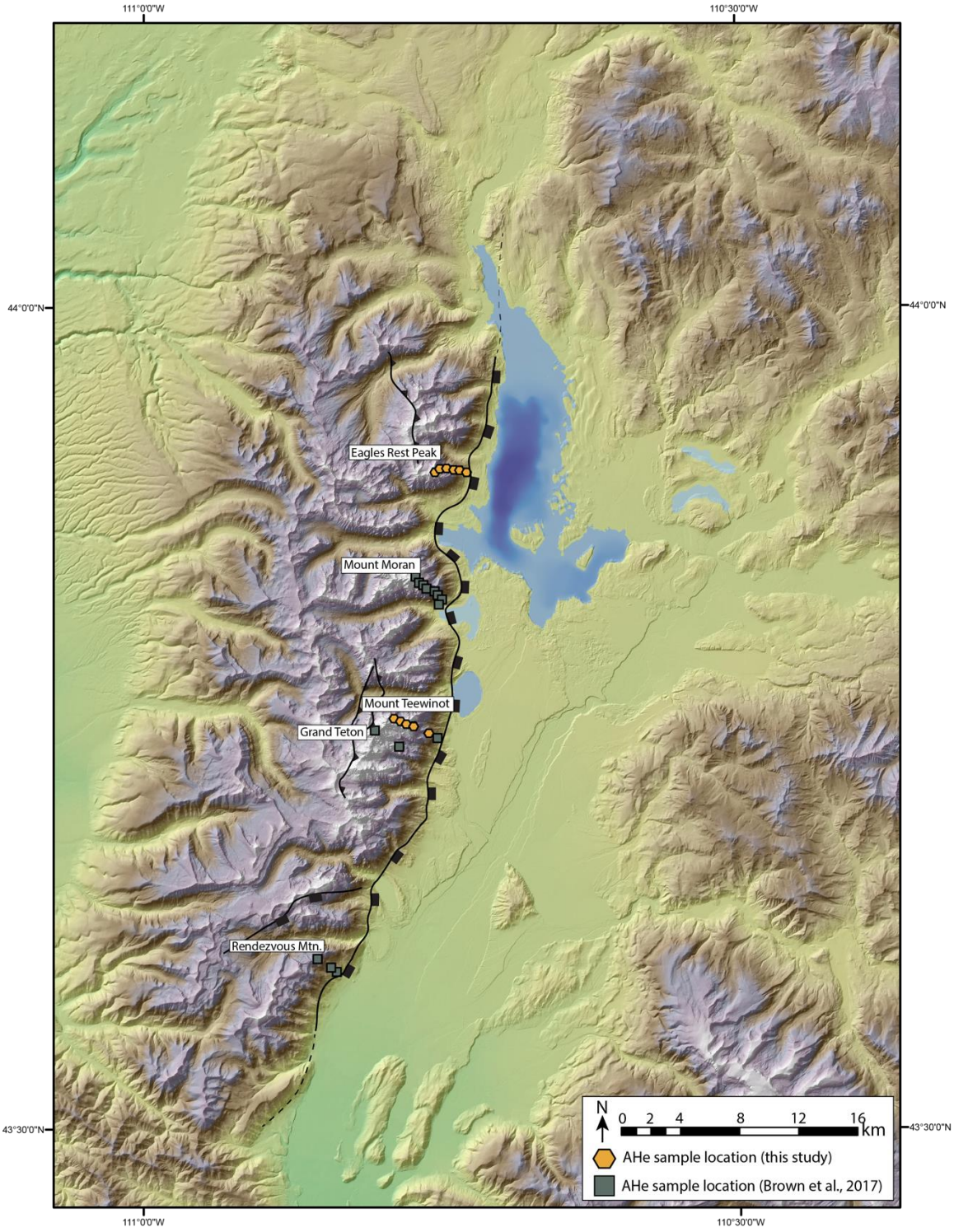

Figure 1.8. Shaded relief map of the Teton Range showing the subvertical sample transects along the eastern Teton range-front. This includes the newly modeled transects in this study at Mt. Teewinot and Eagles Rest Peak as well as those sample-transects modeled in the Brown et al., 2017 study at Mt. Moran, Grand Teton, and Rendezvous Mountain.

2. METHODS

2.1 Low-temperature thermochronology and the apatite-He system

Low-temperature thermochronology, and particularly the apatite and zircon systems, provides constraints for the thermal evolution of rocks in the uppermost crust (Ehlers and Farley, 2003). In particular, systems with the lowest closure temperatures such as the apatite (U-Th-Sm)/He system (AHe; T_c ~70° C) are valuable for understanding near-surface processes such as the timing and rates of fault motion in tectonically active areas (e.g. Armstrong et al., 2003; Braun, 2005). In such studies, AHe and other thermochronologic techniques can yield the cooling history of rocks based on: (1) the empirically and theoretically-predicted t(time)-dependence of He production from radioactive decay of U, Th, and Sm in minerals such as apatite that bear those elements, and (2) the T(temperature)-dependent retention within the grain or diffusion of He out of the grain as a function of T_c (Dodson, 1973; Ketcham, 2005). In regard to mechanism (1), He accumulates within the crystal lattice by the natural decay of ^{238}U, ^{235}U, ^{232}Th, and ^{147}Sm (as well as small amounts of ^{147}Sm), with each isotope having a known rate of decay. This time-dependent process is described by the following equation:

$$\text{Eq. [1]}\ {}^{4}He = 8^{238}U[e^{\lambda 238t}-1] + 7^{235}U[e^{\lambda 235t}-1] + 6^{232}Th[e^{\lambda 232t}-1] + {}^{147}Sm[e^{\lambda 147t}-1]$$

where, ^{4}He, ^{238}U, ^{235}U, ^{232}Th, and ^{147}Sm are the measured amounts of each isotope; λ is the decay constant associated with each isotope; t is the helium age or elapsed time; and coefficients preceding U and Th concentrations represent the number of He-alpha

particles ejected during the decay series (Farley, 2002; Reiners, 2002). Although, this decay scheme is the same for all (U-Th-Sm)/He mineral systems, the T-dependence of He diffusion is mineral system/phase and cooling rate specific. For example, it was found through a series of diffusion experiments by Farley (2000, 2002) that the T_c for the apatite with long grain dimensions ranging from 50-150 μm is ~70°C, assuming a cooling rate of 10°C Ma^{-1}. In (U-Th-Sm)/He systematics, this implies that any He produced within an apatite grain will diffuse readily out of the lattice once the crystal is exposed to temperatures > ~70°C. In contrast, if an apatite grain resides at temperatures significantly below the *Tc* for the AHe system (~40°C), all of the accumulated He within the mineral is retained (Young et al., 1969; Lippolt et al., 1994; Wolf et al., 1996; Warnock et al, 1997; Zietler et al., 1987; Farley, 2000; Ehlers, 2005). Thus, the temperature window from 35-80° C corresponds to the region within the crust known as the apatite partial retention zone (apatite HePRZ or AHePRZ), in which He diffusion out of apatite is variable (Wolf et al., 1998; Farley, 2002). In the context of the apatite-He system, t in Eq. 1 represents the timing or onset age of the most recent cooling event experienced by an apatite grain moving through the upper 1-3 km of the Earth's crust (Fig. 2.1).

In studies involving low-T thermochronology, tectonic processes are not dated directly but rather these analyses date cooling that results from these processes (Ehlers et al., 2001; Stockli, 2005). In normal fault systems such as the Teton fault, AHe ages are interpreted to date footwall exhumation and subsequent cooling that as a result of fault slip-related footwall uplift (Fig. 2.1). In this scenario, the initial onset age of fault slip may be estimated by determining the separation between ages that indicate faster cooling indicative of tectonic processes from those that alternately indicate slower cooling (Fig.

1.5a and 2.1). This technique assumes that the magnitude of fault slip was sufficient to exhume rocks that resided at temperatures above the AHE T_c prior to onset of fault slip (e.g. green circles in Fig. 2.1; Stockli, 2005; Gans et al., 1991; Ehlers and Chapman, 1999). Because the Teton fault is interpreted as a high angle (dip ~60-70°) crustal scale normal fault with a total minimum slip magnitude of ~6 km and a total minimum footwall uplift of ~2 km (Brown et al. 2017), this should result in "unroofing" of at least 2-3 km of the Teton footwall and make application of the AHe technique possible for evaluating the thermal evolution of this system. Furthermore, because the Teton footwall is dominated by favorable lithologies for AHe dating (felsic ortho- and paragneisses), it is possible to document footwall cooling from the base of the range-front to the crest along strategically-targeted subvertical transects. In this way, we are able to quantify both the onset of rapid (fault-related) cooling of the range-front and the rate at which cooling occurred; i.e. the rate of footwall uplift and hence, document the tectonic development of the Teton fault system. Furthermore, since most Basin and Range normal faults depict slip-age distributions along their strike that follows the conventional tip-propagation model of fault growth, in which the oldest ages of slip are located in the fault center and younger ages flanking outwards to the tips (until the age eventually reverts back to older onset age where the tip has not yet broken through), modeled AHe ages collected at locations spanning the entire length of the fault should depict this relationship. Therefore, in this study we conducted AHe analyses for three new subvertical sample transects from the Teton fault footwall, with their specific locations selected to address the questions presented in Chapter 1.

The subvertical sampling strategy reflects the AHe age-elevation sampling approach (Ehlers et al., 2001; Ehlers et al., 2003; Ehlers, 2005). This sampling strategy involves collecting bedrock samples at approximately evenly spaced elevations in the footwall (~200 m apart) to form subvertical sample transects that extend from the base of the range to the crests near the range front (e.g. Fig. 1.5b, 1.5c, 1.5d). By orienting these vertical sample transects normal to the strike of the fault (i.e. parallel to the extensional fault slip direction), each sample along a single vertical transect should be representative of the maximum exposed range of paleodepths in the footwall (Stockli, 2005), assuming that the magnitude of fault slip was enough to exhume footwall rocks from the upper 1-3 km of Earth's crust.

2.2. Study approach

For this research study, we collected and analyzed two subvertical sample transects from the northern, and central parts of the Teton Range at Eagles Rest Peak and Mt. Teewinot, and an additional transect in the southern portion of the Gallatin Range at Dome Mountain (Fig.1.6).

To address whether Mt. Moran is in fact the location of initial motion along the Teton fault or if that location is further north, we collected a new transect 6 km north of the Mt. Moran at Eagles Rest Peak. In addition to the Eagles Rest Peak transect, two additional samples were collected further north from the Gallatin Range. Like the Teton Range, the mountains that compose the Gallatins are bounded along their eastern edge by the N-S striking E-Gallatin normal fault. Since the E-Gallatin fault follows a somewhat similar strike orientation and normal sense of motion with that of the Teton fault (but

lesser magnitude of displacement and present-day relief), then if Mt. Moran or further north is the initial center of the paleo-Teton fault, the AHe ages from the Gallatin samples will be consequential to test the hypothesis suggested by Brown et al (2010, 2017), that the E-Gallatin fault could be the relict northern arm of the paleo-Teton fault prior to emplacement of hotspot volcanism in the region.

In addition to the northern Teton sample transect and the individual samples from Yellowstone, we also collected two sample transects in the central and southern portions of the Tetons to gain further insight on the interpreted increasing rates of slip and younger ages of motion propagating southward along-strike. The location of the Mt. Teewinot transect was chosen because its summit sits directly 2 km east of Grand Teton and thus samples collected along this transect should reveal even more accurate ages of motion at this location along the fault. The southernmost transect of this study, collected at Static Peak was selected because the mountains present farther south along the range are capped by Paleozoic strata which are considered unfavorable for AHe analyses, as indicated by the Brown et al. (2010, 2017) southernmost transect at Rendezvous Mountain having only three interpretable AHe cooling ages.

By using the same methods as those in the related studies of Brown et al. (2010, 2017), we can directly compare our results between these two studies and evaluate the results as whole. In doing so, we aim to provide a more comprehensive understanding of Teton fault structural-tectonic history.

2.3. Analytical procedures

There were a number of incremental processing steps involved to acquire individual apatite grains from each 7-10 kg rock sample. First, each sample was crushed and sieved until all material was reduced to <250 μm diameter grains. Next, materials were processed using a Wilfley table to remove dust and clay-sized particles (<60 μm) and lighter non-ferromagnesian micas from the sample. The large diameter (60-250 μm) Wilfley separate was processed using a gravity filtration apparatus with acetylene tetrabromide (ATB; specific gravity = 2.96 g cc^{-1}) heavy liquid to separate lighter felsic minerals (e.g. quartz and feldspar; specific gravity = ~2.70 g cc^{-1}) from the heavier mafic (e.g. biotite, magnetite, ilmenite, etc.) and U-Th bearing phases (e.g. apatite, zircon, and monazite). The heavy ATB 'sink' phases were magnetically separated using a hand magnet and the remaining separate was processed through a second gravity filtration using methylene iodide (MEI) to separate the denser zircon grains (specific gravity = 4.85 g cc^{-1}) from less dense apatite grains (specific gravity = 3.19 g cc^{-1}). The MEI 'float' was then further processed using a Frantz magnetic separator at progressively increasing amperages of 0.5, 1.0, and 1.8 to separate the completely non-magnetic apatite from other phases. For all samples in this study, density and magnetic separation steps were repeated for each individual sample until they produced enough apatite yield to pick grains for AHe analyses.

For this study, each sample involved picking at least 3-5 single-grain aliquots that were packaged into Nb tubes for U, Th, Sm, and He analyses at the University of Illinois Helium Analysis Laboratory. Individual apatites (single-grain aliquots) were chosen based on grain size (≥ 50 μm grain axial length and radius), shape (ideally euhedral

crystals but fragments can be acceptable), and grain morphology (lack of inclusions, zoning or staining on grain-boundary phases, and preferably free of cracks and imperfections). Identifying the presence of inclusions is critical for these analyses because the inclusion could have its own concentration of He and thus influence the AHe age result. Zircon inclusions in particular pose a problem if they are within an apatite grain that is analyzed for an AHe age. Zircons inclusions affect the overall AHe budget because they can implant their He into the host apatite, yielding an older AHe age. Additionally, because zircons are not dissolved in the dissolution process, the U and Th in the zircon inclusion are not accounted for thus manifesting to an even older and meaningless age for that apatite grain. Therefore, no grains with identifiable inclusions were selected for analyses. For every grain picked, morphological characteristics were also recorded.

In addition to grain morphology, grain-size measurements along both the axial length and radius of each crystal were also recorded This is an important step as grain dimensions (axial length and radius) directly influence the corrections applied to the measured AHe ages. Using step heating experiments of apatite, Dodsen et al. (1973) and Farley (2000) discovered that He diffusion behavior in apatite is dependent on the grain size and radius. Additionally, characterization of grain size is critical for determining the alpha ejection (F_t) correction (Ketcham, 2005 and 2011). When U and Th decay to ^{4}He, the He alpha particle can be ejected from the grain through a high kinetic energy process. In this scenario, He alpha particles produced by U, Th, and Sm atoms that are close enough to the grain boundary (within ~16-20 μm) can lead to the ejection of the He from the grain, thus reducing the calculated age from the AHe measurement. Thus, the size and

dimensions of the grain will dictate whether or not these alpha particles travel completely out of the crystal lattice before coming to rest (Farley et al. 1996). For smaller grains, the percentage of U, Th, and Sm atoms within the ejection range of the grain boundary is much higher and thus the smaller grains require higher F_t correction factors (Ketcham, 2005; Ketcham et al., 2011). This correction accounts for the effects of long-alpha stopping distances (i.e. 20 um for apatite) on AHe ages, assuming a homogeneous distribution of parent isotopes within each individual mineral. Once the diffusion and ejection corrections are made to the AHe ages, the closure temperature can be calculated for each sample using the following equation by Harrison and Zeitler (2005):

$$\text{Eq. [2]} \quad Tc = (E/R) / \ln[(ARTc^2D_0/a^2)/(E\mathit{dt}/\mathit{dt})]$$

where E is the 33 kcal/mol activation energy (Farley, 2000), R is the universal gas constant, A is the shape factor of 55 for an infinite cylinder (Dodson, 1973), D_0 is the He diffusivity at infinite temperatures (50 cm^2s^{-1}) (Farley, 2000), a is the radius of the crystal diffusion domain, and dT/dT is the cooling rate (10°C Ma^{-1}; Farley, 2000 and 2002).

The AHe analyses for this study were completed at the University of Illinois-Urbana Champaign (UIUC) Helium Analysis Lab (HAL) and the Radiogenic Helium Dating Lab at the University of Arizona. To derive the measured AHe ages for our sample suite, we measured the isotope concentrations associated with each aliquot by the standard techniques described in Farley (2000). First, each grain was outgassed for He using an in-vacuum extraction line that is heated with Nd:YAG, CO_2 or diode laser. The heating schedule was approximately 950-1050°C for 3 minutes for each aliquot. After

^{4}He has been extracted from the crystal domain it is spiked with ^{3}He, purified using cryogenic and gettering methods, and analyzed on a quadrupole mass spectrometer (QMS). A known quantity of ^{4}He is present throughout the entire analysis schedule to monitor instrument sensitivity as well as Durango fluroapatite gas standards are run every 4th apatite that is analyzed throughout the duration of the analysis schedule. Following ^{4}He outgassing and purification, the degassed aliquots are retrieved from the Nb packets and dissolved in HNO_3 at 90°C for one hour. After dissolution, the aliquots were equilibrated and spiked with ^{223}U-^{229}Th-^{147}Nd-^{42}Ca and U, Th, and Sm concentrations were measured with a Thermo iCAP Q ICP-MS. These isotope abundances were then applied to Eq. [1] along with the measured He to solve for the raw AHe age, i.e. t in Eq. [1]. Important to note is that the measured He from each grain is blank corrected, such that it compares to what the He value of known quantity is when a blank (empty) aliquot is run through the analyses. If values are a few times greater than blank, then this correction becomes too large and renders this age meaningless. Thus, although there were at least three apatites analyzed per every sample, some of the grains with near blank values of He had to be culled from the dataset.

2.4. Data analyses: time-temperature (t-T) cooling histories

The final step of our analyses was to produce inverse thermal history models for each subvertical transect using QTQt. The QTQt program uses a Bayesian Markov Chain Monte Carlo (MCMC) algorithm, in which the model takes repeated random walks through the model space to construct a posterior probability distribution of possible T-t paths given input data (AHe age, sample elevation, and present-day temperature, etc.)

(Gallagher, 2012; Vermeesch and Tian, 2014). We assumed a modern geothermal gradient of 30° C km^{-1} and accounted for variation in aliquot size and morphology (infinite cylinder, grain fragment, or sphere) by applying the appropriate diffusion models to correct for the laboratory measured AHe ages prior to running each model simulation. Tables 1 (Mt. Teewinot transect), Table 2 (Eagles Rest Peak transect), and Table 3 (Dome Mountain transect) provides the corrected ages utilized and the inputs associated with each of the T-t history models generated in this study.

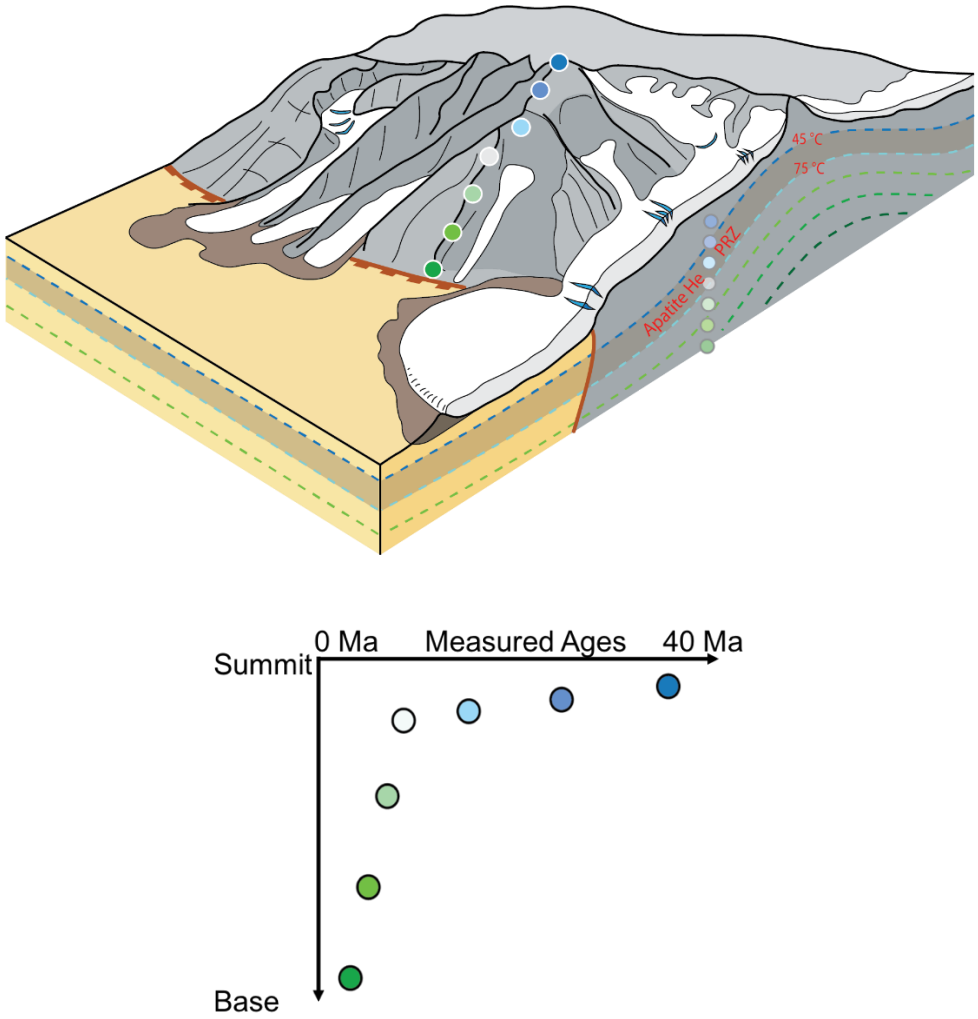

Figure 2.1. Conceptual block model of a normal faulting and the AHe age-elevation method. This figure reflects how AHe-analyses of samples collected along subvertical transects in the footwall of a normal fault can reveal the thermal history of those samples. In AHe dating, as the apatites in these rock samples pass through the AHe partial retention zone in response to faulting and exhumation, He within the apatite will start to become retained inside the grain. By determining the relative amounts of He to the parent U and Th atoms within an apatite we can determine the time at which these rocks experienced the event that caused them to cool and retain He. By plotting AHe ages for samples collected along subvertical transects with respect to the elevations that they were taken, a cooling history for those samples as they passed through the upper crust (1-3 km) can be inferred. In ideal circumstances, AHe ages from the samples collected along each footwall transect will decrease from the summit to the base of the range front. Furthermore, in simple normal fault systems, the break in slope shown in the AHe age-elevation plot (occurring at the white circle) will identify the onset time at which the footwall rocks went from non-tectonic (erosion-related cooling) to tectonic (fault-related cooling) Modified from Thigpen et al. (2018).

3. RESULTS

3.1. AHe Results

In this study, AHe ages from all individual apatites collected from the Teewinot, Eagles Rest, and Dome Mountain (Gallatin) transects range from 93.3 Ma to 5.78 Ma (Tables 1.1, 1.2, 1.3). In this section, we report the average calculated ages and standard deviation for each sample along each transect.

Along the southernmost transect collected by this study at Teewinot (Fig.1.5), AHe ages averaged from multiple aliquots at each sample locality (Table 1.1) ranged from 35.9 ± 9.3 to 8.1 ± 0.3 Ma over an elevation range of ~1000 m, from 3102 to 2185 m. Sample TR-16-01, which initially yielded the oldest average age along the transect (38.7 ± 30.1 Ma) at an elevation of 2997 m was culled from the dataset due to the large error produced by averaging individual AHe aliquot ages of 60.04 and 17.41 Ma. At an intermediate elevation, sample TR-16-07 (2787 m) produced an average AHe age of 22.9 ± 7.8 Ma. Unfortunately, intermediate elevation samples TR-17-07 (2682 m), TR-16-08 (2420 m), and TR-16-09 (2185 m) produced near blank levels of He during analysis and were thus also culled from the dataset, producing a significant data gap in the transect that will be discussed later.

Along the Eagles Rest Peak transect (Fig.1.7), average AHe ages from samples collected 300 m below the summit (TR-17-09; elev. 3120 m) to the lowest exposed bedrock outcrop (TR-17-14; elev. 2362) range from 95.5 ± 2.90 Ma to 5.78 ± 0.16 Ma. The highest elevation sample along the Eagles Rest transect yields a single AHe age of 93.25 ± 1.87 Ma. Intermediate elevation samples TR-17-10 (elev. 2972), TR-17-11 (elev.

2823), and TR-17-12 (elev. 2607) yield average AHe ages of 81.8 ± 7.7 Ma, 34.9 ± 25.5 Ma, and 7.4 ± 1.2 Ma, respectively. Another intermediate elevation sample, TR-17-13, yielded near blank level He during analysis and was thus culled from the dataset. Sample TR-17-14 (elev. 2362), which is the lowest elevation sample collected along this transect, shows an apparent inversion with an age of 14.6 ± 2.7 Ma.

Lastly, in the Gallatin Range north of Yellowstone, two samples collected near the base of Dome Mountain yield ages ranging from 18.94 ± 7.68 Ma to 8.23 ± 2.06 Ma. The highest elevation sample, TR-17-16 (elev. 2708), yields an average AHe age of 14.0 ± 7.0 Ma from two aliquots that yield single grain ages of 18.94 ± 7.68 and 9.02 ± 3.06 Ma. The lowest elevation sample, TR-17-15 (elev. 2628), yields an average AHe age of 12.3 ± 3.0 Ma from five single grain aliquot ages. Due to the limited accessible exposure, only two samples were collected along this transect.

3.2. Inverse Thermal History Models

Multi-sample inverse thermal history models were produced for the Eagles Rest and Teewinot transects to examine the possible range for Teton fault slip onset ages near each of these subvertical transects (Figs. 4.1 and 4.2). An additional inverse thermal history model was produced for the Dome Mountain transect in the Gallatin Range in northern Yellowstone to assess the uplift history along the E-Gallatin fault. The latter model was intended to test the speculative hypothesis put forth by Brown et al. (2017) that the East Gallatin normal fault may represent a segment of the Teton fault that was separated from the main Teton fault by migration of the Yellowstone Hotspot into the region at ~2 Ma. Here, each thermal history model for the samples associated with each

respective transect represent the AHe age and error from each individual apatite grain per sample.

At Eagles Rest, integrated modeling of 14 single-grain aliquots associated with five samples predicts a protracted period of slow post-Laramide cooling followed by a period of rapid cooing (24°C Myr^{-1}) from 9 to 7 Ma and then a reduction of cooling rate (7°C Myr^{-1}) from 7 Ma to present (Fig. 4.1). To the south at the Mt. Teewinot transect, inverse thermal history modeling 17 single grain aliquots for 6 samples (Fig. 4.2) yields a post-Laramide cooling history with an uplift onset at 32 Ma, with a long-term cooling rate of ~2 °C Myr^{-1}. North of Yellowstone, inverse thermal history modeling of 7 single grain aliquots from two samples yields an uplift age of 16-10 Ma during a period of relatively slow cooling (~2.4°C Myr^{-1}). This is followed by increased cooling (~5.8°C Myr^{-1}) from 10 Ma to present.

Table 1.1. Apatite-He dataset for the Mt. Teewinot transect

Teewinot Transect													
Sample	**Elev (m)**	**Length (μm)**	**Width (μm)**	**He (pmol)**	**U (ppm)**	**Th (ppm)**	**eU (ppm)**	**Sm (ppm)**	**Raw Age**	**Corrected Age**	**Error**	**Avg Age**	**Std Dev**
TR-16-05-01	3103	140.3	95.2	0.0521	104.1	56.2	117.3	477.4	24.10	31.39	0.84	**35.9**	9.3
TR-16-05-03		196.6	119.2	0.0179	18.3	7.8	20.1	268.1	19.88	24.98	1.02		
TR-16-05-04		159.4	90.4	0.0286	33.6	22.2	38.8	330.3	33.35	43.44	1.15		
TR-16-05-05		168.2	85.1	0.0128	14.8	7.0	16.4	228.1	33.83	43.83	1.35		
TR-16-06-01	2998	71.5	69.1	0.0055	35.5	22.4	40.7	335.9	34.38	60.04	2.63	**30.0**	30.1
TR-16-06-03		120.9	68.3	0.0015	12.8	4.8	14.0	79.5	12.10	17.41	1.48		
TR-16-07-05	2787	119.0	67.8	0.0047	27.6	1.8	28.0	170.6	18.44	25.82	1.95	**22.9**	7.8
TR-16-07-06		167.9	62.7	0.0032	15.0	1.0	15.2	120.7	12.03	16.52	1.00		
TR-16-07-07		100.4	74.5	0.0071	40.2	5.1	41.3	231.0	23.65	34.97	1.51		
TR-16-07-08		72.9	54.2	0.0005	26.3	-16.1	22.5	212.6	9.09	16.46	5.09		
TR-16-07-09		91.2	73.5	0.0030	41.0	-3.5	40.1	252.7	13.29	20.61	0.83		
TR-17-07-01	2682	99.0	78.0	0.0029	31.5	-2.1	31.0	179.4	13.74	20.69	1.56	**20.7**	0.0
TR-16-09-03	2185	132.0	114.3	0.0088	57.7	36.6	66.3	7.1	6.17	8.05	0.31		
TR-08-23A	2130	141.8	80.5	0.0219	58.3	13.4	61.4	N/A	5.96	7.11		**6.8**	0.4
TR-08-23B		130.6	90.2	0.0133	41.8	6.9	43.4	N/A	5.21	6.28			
TR-08-23C		115.0	67.2	0.0060	37.1	5.9	38.5	N/A	5.46	6.83			
TR-08-23D		166.5	115.9	0.0235	29.4	3.1	30.1	N/A	6.03	7.03			

Table 1.2. Apatite-He dataset for the Eagles Rest Peak transect

Eagles Rest Peak Transect													
Sample	Elev (m)	Length (um)	Width (um)	He (pmol)	U (ppm)	Th (ppm)	eU (ppm)	Sm (ppm)	Raw Age	Corrected Age	Error	Avg Age	Std Dev
TR-17-09-03	3120	108.9	82.7	0.0321	43.2	7.3	44.9	93.3	63.51	93.25	1.87	**93.3**	0.0
TR-17-10-04	2973	77.2	61.0	0.0112	74.1	9.7	76.4	89.5	45.66	78.75	2.47	**81.8**	7.7
TR-17-10-05		113.2	70.2	0.0139	42.3	6.8	43.9	91.2	50.32	78.45	2.20		
TR-17-10-06		98.1	71.0	0.0134	38.7	3.6	39.6	59.7	60.91	95.47	2.90		
TR-17-10-07		84.7	60.1	0.0142	91.0	6.1	92.5	225.8	44.65	76.61	2.96		
TR-17-10-08		60.1	48.5	0.0061	104.4	22.2	109.6	142.7	39.63	79.77	3.35		
TR-17-11-01	2823	154.4	62.8	0.0053	16.1	9.5	18.3	215.4	32.87	52.90	0.72	**34.9**	25.5
TR-17-11-02		103.0	82.8	0.0011	7.9	8.1	9.8	225.1	10.96	16.90	0.27		
TR-17-12-02	2607	104.0	67.1	0.0003	14.2	1.7	14.6	35.4	3.46	5.78	0.16	**7.4**	1.2
TR-17-12-04		76.7	50.3	0.0002	14.4	7.1	16.1	22.6	3.88	7.57	0.28		
TR-17-12-06		125.7	65.3	0.0004	11.0	2.5	11.6	28.5	4.51	7.49	0.19		
TR-17-12-07		71.8	50.0	0.0002	13.4	6.0	14.8	22.5	4.09	8.62	0.68		
TR-17-14-01	2362	103.1	57.8	0.0004	7.9	5.6	9.2	85.2	9.54	16.55	0.66	**14.6**	2.7
TR-17-14-02		141.8	63.9	0.0007	9.2	7.6	11.0	97.9	7.64	12.71	0.49		

Table 1.3. Apatite-He dataset for the Dome Mountain transect

Dome Mountain Transect													
Sample	**Elev (m)**	**Length (um)**	**Width (um)**	**He (pmol)**	**U (ppm)**	**Th (ppm)**	**eU (ppm)**	**Sm (ppm)**	**Raw Age**	**Corrected Age**	**Error**	**Avg Age**	**Std Dev**
TR-17-16-02	2708	84.6	62.1	0.0004	6.1	14.7	9.5	373.1	10.53	18.94	7.68	**14.0**	7.0
TR-17-16-03		80.8	74.3	0.0004	11.5	11.7	14.3	250.9	5.72	9.02	3.06		
TR-17-15-01	2628	235.4	182.8	0.0085	6.0	3.3	6.8	107.0	12.13	14.14	0.52	**12.3**	3.0
TR-17-15-02		97.7	82.5	0.0004	6.6	5.8	7.9	109.6	5.39	8.23	2.05		
TR-17-15-03		102.8	59.0	0.0008	7.5	17.6	11.7	96.0	10.50	16.12	2.73		
TR-17-15-04		129.9	87.8	0.0007	4.0	7.3	5.7	93.6	8.51	11.84	1.80		
TR-17-15-06		102.5	52.5	0.0002	4.7	6.4	6.2	139.0	6.70	10.97	5.02		

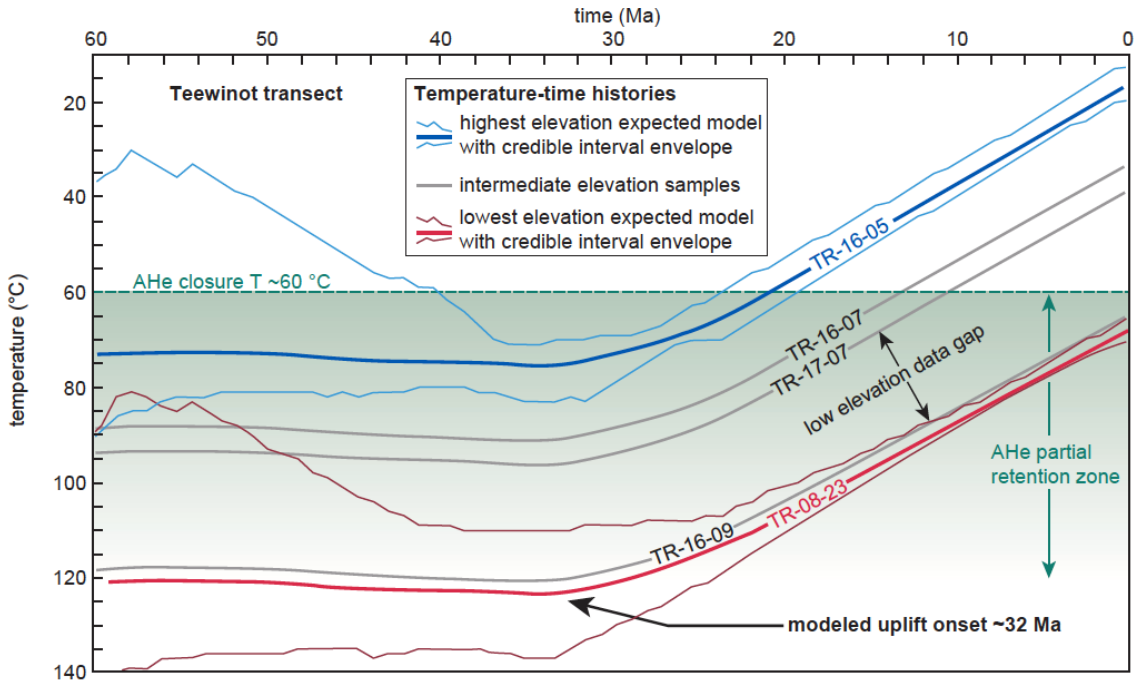

Figure 3.1. QTQt inverse thermal history model produced from the measured AHe ages for samples collected along the MT. Teewinot transect. Modeled onset of uplift at 32 Ma. Note the low-elevation data gap, and thus caution should be advised in interpretations of this age.

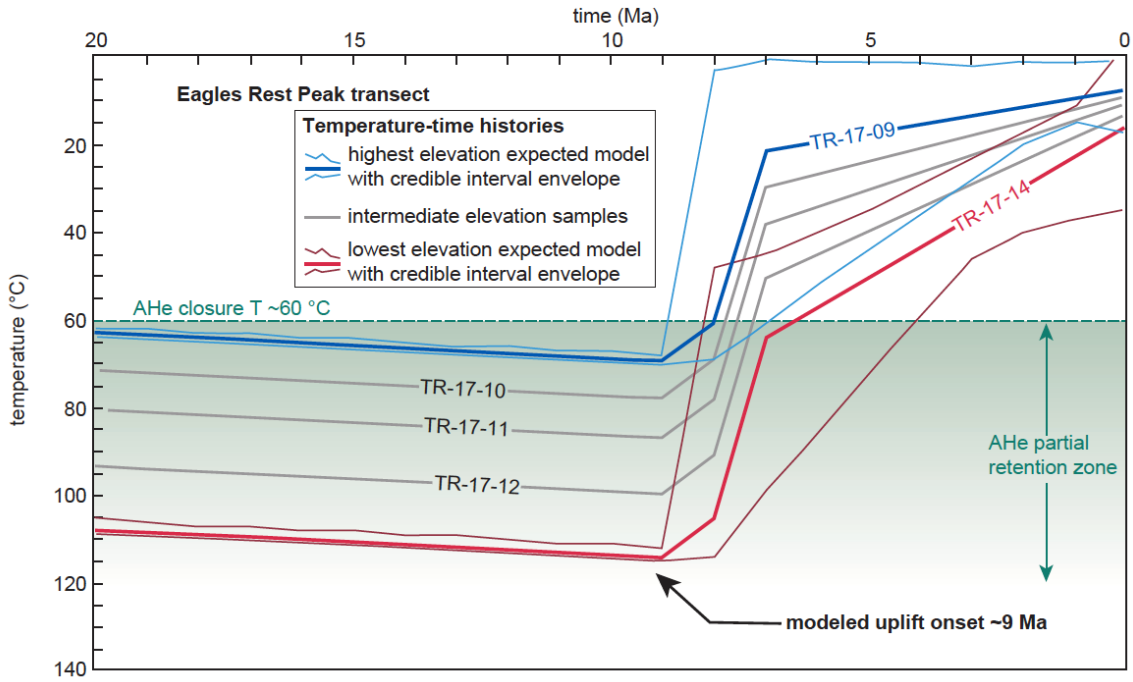

Figure 3.2. QTQt inverse thermal history model produced from the measured AHe ages for samples collected along the Eagles Rest Peak transect. Modeled onset of uplift-related footwall cooling at approximately 9 Ma at this location along the range front.

4. DISCUSSION

4.1. Slip onset and uplift for the northern Teton fault at Eagles Rest Peak

Brown et al. (2017) originally hypothesized that the approximate center of the Teton fault could either be near Mt. Moran or further north based on AHe model results that indicated a progressive southward younging of fault slip onset from Mount Moran in the north (13-15 Ma), to the Grand Teton (~10 Ma) at the traditionally interpreted fault center, and finally to Rendezvous Peak (~7 Ma) in the southern part of the range. For each transect in the Brown et al. (2017) study, 'modeled' ages incorporated into the inverse thermal history models show excellent agreement with measured ages (Fig. 4.1). If the center of the Teton fault does indeed lie in the vicinity of Mount Moran fault slip onset ages should also get younger to the north of Mount Moran, as predicted by theoretical models of fault growth (Kim and Sanderson, 2005). Alternately, if the true center of the Teton fault is north of Mount Moran, fault slip onset ages determined from analysis of subvertical transects north of Mount Moran should yield older (i.e. >13 Ma) fault slip onset ages.

At Eagles Rest Peak ~6 km north of Mount Moran, inverse thermal history modeling indicates rapid fault-related cooling (~24°C Myr^{-1}) began at ~9 Ma and lasted until ~7 Ma, followed by a deceleration in cooling rate (~7°C Myr^{-1}) that has continued to present-day (Fig. 4.2). Like the results of Brown et al. (2017), our results show excellent agreement between measured and modeled AHe ages (Figs. 5.1a and 5.2b). Thus, the younging age trend recognized south of Mt. Moran is mirrored to the north along the Eagles Rest transect reported here, supporting the interpretation put forth by Brown et al.

(2017) that Mt. Moran could likely represent the location along strike where slip along the Teton fault first initiated.

4.2. Northern extension of the Teton fault

If the center of the Teton fault is indeed located in the vicinity of Mount Moran, it is useful to consider how far north the Teton fault potentially extended prior to encroachment of the Yellowstone hotspot into its present-day position at ~2 Ma. By combining theoretical models of normal fault growth via tip propagation with empirical observations of fault length-displacement relationships, it is possible to predict how these structures accommodate displacement and extend outwards from center where slip first initiates. Fault length-displacement scaling reveal a clear relationship between the mappable trace length of the fault (L) and maximum accumulated displacement (D or D_{max}; Bergen and Shaw 2010), with most normal faults yielding an observed L:D of ~15:1 to 30:1 (Fig. ; Densmore et al. 2004; Bergen and Shaw 2010;).

For the Teton fault, Brown et al. (2017) proposed a minimum estimate for maximum displacement of ~6 km at Mount Moran by combining footwall uplift magnitudes from thermochronology (~2 km) with numerical models of normal fault systems, wherein footwall uplift represents ~33% of the total displacement (Thompson and Parsons 2009). If the Teton fault follows the commonly recognized scaling relationships, a Dmax of ~6 km should produce a total minimum mapped length of 100-180 km for the Teton fault (Brown et al. 2017) (Fig. 1.8), substantially longer than the 70 km length traditionally inferred from the footwall topography and geologic mapping (Love, 1977; Love et al., 2003). Assuming that the Teton fault center is at Mount Moran

then the fault should extend 50-90 km north and south of the Moran region (Fig, 1.7). To the south, the Teton fault is mapped as terminating against the Cache Creek thrust ~45 km south of Mount Moran (Fig. 1.1d; Love, 1977; Love et al., 2003). Because this termination is a more complex kinematic scenario than that assumed in simple tip propagation models, it is possible that the southern extension of the fault does not behave in the theoretically predicted manner. To the north, a 50-90 km would place the northern extent of the Teton fault in northern Yellowstone in vicinity of Lewis Lake at minimum and possibly as far north as the northernmost extent of Yellowstone Lake. Additionally, although preliminary work is currently underway, a northern extension of the Teton fault is supported by studies of modern (Quaternary) fault scarp offsets of up to 12 m imaged north of Jackson Lake by LiDAR (National Park Service, 2014) and by recent lake seismic reflection surveys that show linkage between these disparate northern fault scarps and the main trace of the Teton fault (Thigpen et al., 2018; Thigpen et al., in prep).

4.3. Possible linkages between the Teton and Gallatin Range normal faults

Because Brown et al. (2017), originally proposed that the Teton fault could possibly extend into northern Yellowstone and be kinematically linked with the East Gallatin normal fault, this study also collected AHe data from the Gallatin region to test this idea. In this scenario, the East Gallatin fault, which has a similar strike as the Teton fault, could potentially represent a vestigial segment of the paleo-Teton fault that was separated from the main Teton fault segment to the south by encroachment of the Yellowstone hotspot into the region at ~2 Ma (Brown et al. 2017). Although our data from Eagles Rest peak combined with the Brown et al. (2017) data from Mount Moran

seems to preclude the possibility that these two structures were originally a single structure, it is interesting to consider if they are of approximately the same age and thus may be kinematically linked along a greater regional crustal trend. To test this hypothesis, we collected the Dome Mountain transect in the southern Gallatin Range (Fig. 1.6). Inverse thermal history models for this transect, although composed of only two samples spaced ~100 vertical m apart, reveal that uplift related cooling (~2.4°C Myr^{-1}) began at ~16 Ma followed by accelerated cooling (~5.8°C Myr^{-1}) from ~10 Ma to the present (Fig. 1.6c and 4.2c). If correct, the similarity of motion onset ages of the Teton (13-15 Ma) and Gallatin (~16 Ma) faults combined with their similar structural trend suggests that these faults may be part of the same larger crustal lineament of extension within the regional system. Certainly, additional work would need to be performed to further develop this hypothesis, but it remains an interesting possibility nonetheless.

4.4. Uplift history of the Teewinot transect and comparison with Teton fault evolution models

Most of the current study focused on further constraining the evolution of the northern extent of the Teton fault. However, both of the models for the central and southern segments of the fault (Grand Teton and Rendezvous) included in Brown et al. (2017) dataset only included three samples each. To address this in the central part of the range, we collected the Teewinot transect. Because Teewinot is positioned approximately adjacent to the projected fault surface in front of the Grand Teton and has a steeper elevation gradient, we considered that samples collected along the Teewinot transect

should provide a more accurate representation of fault motion than the Grand Teton transect of Brown et al. (2017).

Using inverse thermal history modeling, the Teewinot transect produced the oldest fault slip onset age (~32 Ma) and the slowest cooling rate (~2°C Myr^{-1}) yet observed from any of the transects in the current study or those of Brown et al. (2017). This result yields two possible scenarios; either motion on the Teton fault is much older than that indicated by models from four other fault transects of Brown et al. (2017) and this study or, the Teewinot model does not reflect the actual fault slip history. To evaluate these scenarios, we first examined the agreement between the modeled and observed AHe ages of Brown et al. (2017) for the Rendezvous and Grand Teton transects (Fig. 4.2 a and b). In each instance, differences between the observed and modeled ages never exceed ~2 Myr for the critical samples located along the lower to mid-elevations in each transect. This is also the case for the Mount Moran model, with the highest elevation samples showing the only major divergence (~8 Myr) of modeled and observed ages. This suggests that, despite the limited number of samples, these models are robust. This is also true for the Eagles Rest Peak transect in the current study, wherein modeled ages generally follow the observed age trend, with the exception of sample TR-17-11, which shows a very large range of observed ages. The Eagles Rest transect is also anchored by sample TR-17-12, which yields one of the best 'averaged' ages in the entire dataset (7.4 ± 1.2 Ma) and is the critical sample that drives the model to a fault slip onset age of ~9 Ma.

In the Teewinot transect, the modeled fault onset age of ~32 Ma is driven by an age-elevation inflection point created by sample TR-16-06, which produced only two aliquot ages of 60.04 ± 2.63 Ma and 17.41 ± 1.48 Ma. Reasoning for the wide spread in

ages could likely be attributed to the understanding that because this sample was collected at a higher elevation, it is likely that the aliquots were resting above or within the PRZ at the time of exhumation leading to differences in He retention in these aliquots and thus the resulting ages. These two aliquots produce an essentially meaningless 'average' age of 38.7 + 30.1 that drives the model to produce the very early onset age. To address this, we removed sample TR-16-06 and ran a second inverse thermal history model (Fig. 4.3) that produced a fault slip onset age of ~23 Ma. In this revised model, which still yields an age much older than the other transects, the onset of uplift in the model is driven by the inflection point produced by samples TR-16-07 and TR-17-07 between the oldest and youngest samples in the transect. Although sample TR-16-07 had five aliquots for the model to project through, TR-17-07 only had one aliquot. Had TR-17-07 had more aliquots, the model path would likely alter and therefore it is important to be cautious in interpreting ages from samples with less than three aliquots. This was the case for samples collected between TR-17-07 and the lowest elevation samples (TR-16-09 and TR-08-23), which yielded near blank levels of He in all analyses, and thus were necessarily culled from the current dataset. This data absence created an ~500 m segment of no data along the transect, and thus we have chosen to consider models produced by the transect as suspect until more analyses can be run for this missing samples. We consider this cautious approach to the Teewinot transect results to be particularly prudent as it is currently incompatible with all other models produced both by this study and Brown et al. (2017). With this caution in mind, we have not eliminated the possibility that this part of the fault is indeed older than proposed by Brown et al. (2017), but future work will have to address this possibility.

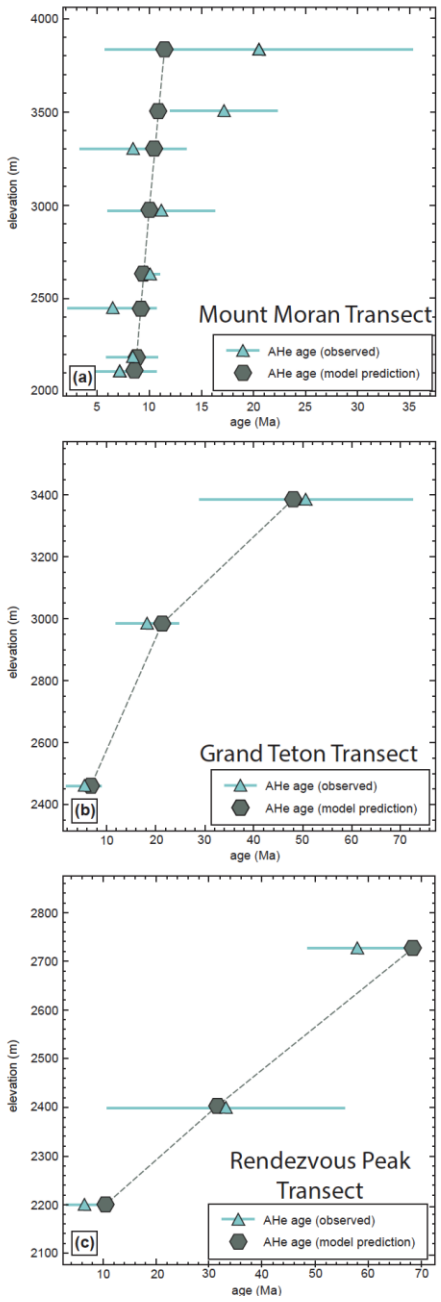

Figure 4.1. Age elevation gradient plots that describe the relationship between the measured ages and the model results for the most likely thermal history that the suite of samples along each transect from the Brown et al., study that reveals a southward younging in motion ages across the Teton fault. This is supported in these plots as the modeled and the measured ages coincide with each other.

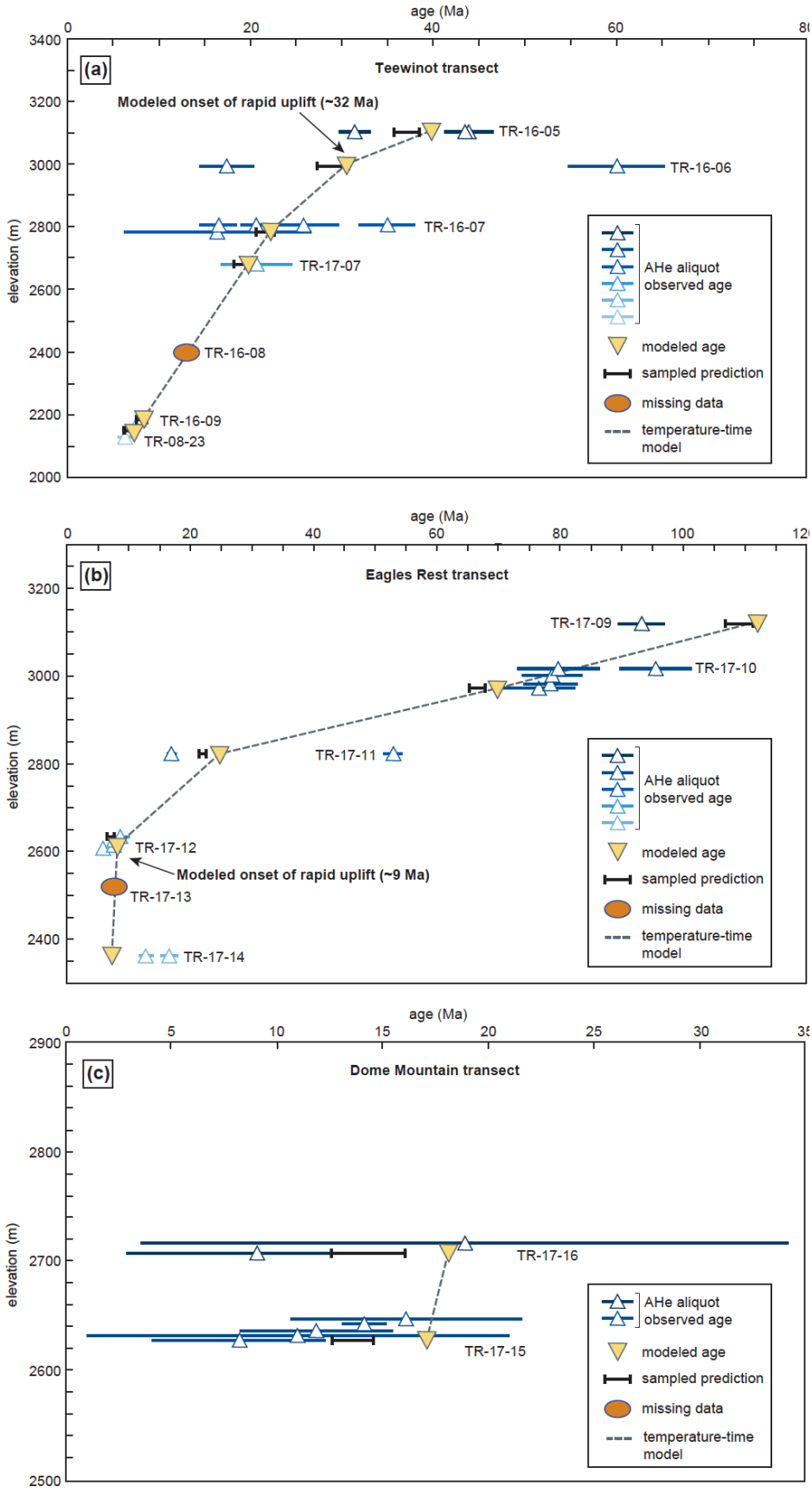
(a)
Teewinot transect
Modeled onset of rapid uplift (~32 Ma)
TR-16-05
TR-16-06
TR-16-07
TR-17-07
TR-16-08
TR-16-09
TR-08-23
AHe aliquot observed age
modeled age
sampled prediction
missing data
temperature-time model
age (Ma)
elevation (m)
(b)
Eagles Rest transect
TR-17-09
TR-17-10
TR-17-11
TR-17-12
Modeled onset of rapid uplift (~9 Ma)
TR-17-13
TR-17-14
(c)
Dome Mountain transect
TR-17-16
TR-17-15

Figure 4.2. Age elevation gradient plots that describe the relationship between the measured ages and the model results for the most likely thermal history that the suite of samples along each transect went through in response to fast-cooling from fault slip-onset and exhumation of the range-front. The good agreement between the measured and modeled ages yields confidence in the model prediction, while bad agreement is preceded with some necessary caution and should not be overinterpreted.

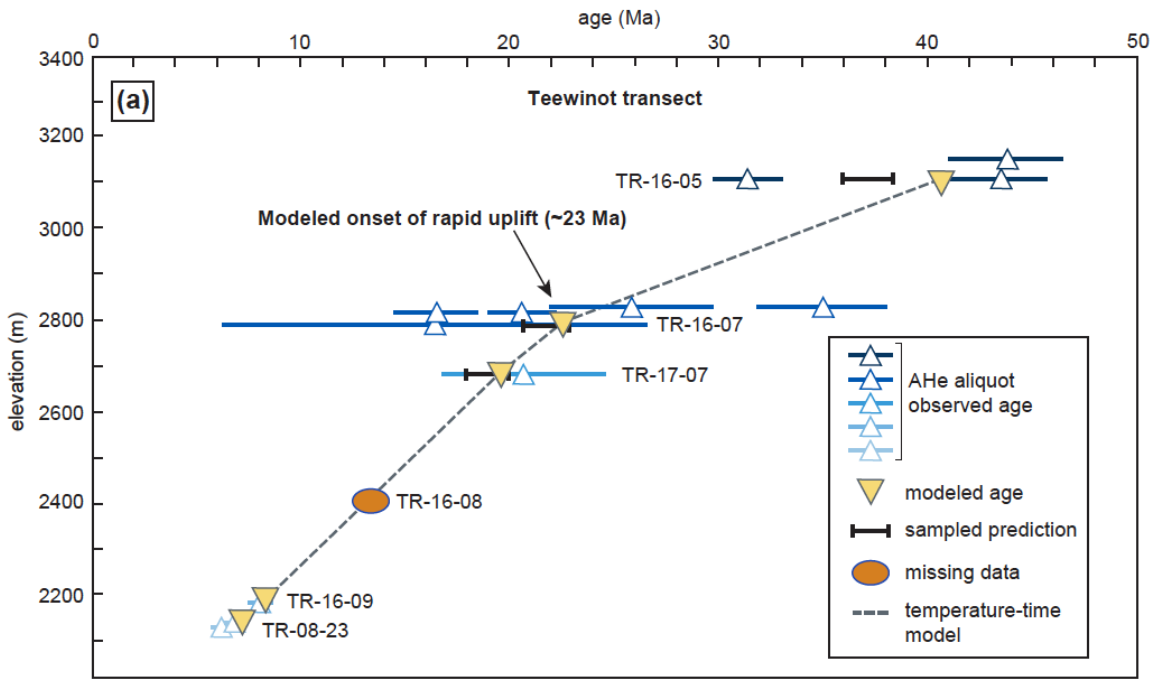

Figure 4.3. New Mt. Teewinot age-elevation gradient. This new Teewinot age-elevation plot shows that when the only aliquots from sample TR-16-06 with ages of 60.04 ± 2.63 Ma and 17.41 ± 1.48 Ma are removed due to their meaningless averaged age, we see that the onset age of faulting (or inflection point) is younger at 23 Ma. We interpret this age as a maximum fault onset age because gap between where the model puts this new inflection point and the lowest elevation samples, would likely have onset ages of 23 Ma or younger. Nevertheless, we present the Teewinot results with caution in our interpretations as much more data is needed for Mt. Teewinot to refine the uplift history along the Teton fault at this location.

5. CONCLUSIONS

New AHe ages derived from the footwalls of the Teton and East Gallatin faults yield new constraints on development of normal fault systems in the greater Teton-Yellowstone region. These datasets particularly provide insight into the evolution of the northernmost extent of the Teton fault and possible dynamic linkages with the East Gallatin fault north of Yellowstone. In the northernmost part of the Teton Range, AHe ages from a subvertical transect collected at Eagles Rest Peak range from 95.5 ± 2.90 Ma to 5.78 ± 0.16 Ma. An inverse thermal history model of this transect indicates that rapid fault-related cooling (~24°C Myr^{-1}) began at ~9 Ma and lasted until ~7 Ma, followed by a deceleration in cooling rate (~7°C Myr^{-1}) that has continued to present-day. In comparison, the Brown et al. (2017) transect located ~6 km south of Eagles Rest Peak at Mount Moran showed an older onset uplift age of 13-15 Ma. Farther south of Mt. Moran, the Brown et al. (2017) transects at the Grand Teton and the southernmost transect at Rendezvous Peak reveal fault slip onset ages that become progressively younger (10 and 7 Ma, respectively). Modeled AHe ages from all four of these transects (Eagles Rest Peak, Mt. Moran, Grand Teton, and Rendezvous Peak) show excellent agreement with the measured ages. Evidence of a southward-younging age trend, originating at Mt. Moran in the Brown et al. (2017) dataset, and a corresponding northward trend along the Eagles Rest Peak transect reported from this study corroborates the interpretation made by Brown et al. (2017) that Mount Moran may represent the locus of initial fault slip initiation along the Teton fault. If the Teton fault behaves according to a conventional tip-

propagation model of normal fault growth, Mt. Moran can be reasonably interpreted as the center of the fault.

If Mount Moran is considered to be the center of the Teton fault, fault length-displacement (L:D) scaling relationships can be used to predict the potential northernmost extension of the Teton fault prior to encroachment of the Yellowstone hotspot into its present-day position at ~2 Ma. Brown et al. (2017) determined that the Teton fault has accumulated a minimum of ~6 km of displacement at Mt. Moran and, thus yielding a total mapped length of 100-180 km, assuming that the Teton fault falls within L:D ratios of 15:1 to 30:1 as observed in most normal fault systems. If we assume that Mount Moran represents the center of the fault based on this study and the work of Brown et al. (2017) then the fault should extend 50-90 km north and south of the Moran region. The mapped southern boundary of the Teton fault intersects the Cache Creek thrust, where the fault is suspected to terminate. Because of the kinematic complexity of this southern termination, it is possible that the southern extension of the fault does not behave in the theoretically predicted matter. That interaction is beyond the scope of this study and will be the focus of future work. To the north, a 50-90 km extension of the fault would place the northernmost tip of the Teton fault within the area near Lewis Lake in central Yellowstone (50 km extension) or even as far as north of Yellowstone Lake (90 km extension). Preliminary studies of Thigpen et al. (2018) and Thigpen et al. (in prep) reveal modern (Quaternary) fault scarp offsets of up to 12 m observed in LiDAR data north of Jackson Lake (National Park Service, 2014). Also, recent lake seismic reflection surveys from the aforementioned studies show linkage between the disparate northern fault scarps and the main trace of the Teton fault (Thigpen et al. 2018), which further

supports the northern extension of the Teton fault proposed here. Although Brown et al. (2017) originally suggested that the Teton and East Gallatin faults may have been linked prior to encroachment of the Yellowstone hotspot into its present-day position, this work now precludes that interpretation. Despite this, new AHe ages from the Gallatin Range reported here yield a fault slip onset of ~16 Ma, and thus the similar age and trend of the East Gallatin and Teton faults suggests that they might be dynamically linked along regional crustal extensional lineament.

The largest discrepancy in the data presented for this study is from the Mt. Teewinot transect. The thermal model for the Teewinot transect produces the oldest onset age of ~32 Ma and the slowest cooling rate (~2°C Myr^{-1}). This early onset age and slow cooling rate produces two likely scenarios: (1) motion along the Teton fault is much older than that indicated by the combined model results from our transect at Eagles Rest Peak and the three transects from the Brown et al. (2017) study or, (2) the Mt. Teewinot model does not reflect the actual slip history. An evaluation of the Teewinot model shows that the ~32 Ma onset age is driven by a modeled inflection point that averages two aliquots of 60.04 ± 2.63 Ma and 17.41 ± 1.48 Ma from a single sample. If this age is culled from the dataset, inverse thermal history modeling yields an onset age of ~23 Ma. This onset age, which is still older than the other transects, is determined by two samples that lie between the oldest and youngest ages along the transect. The position of these two samples from the youngest samples at the base of the transect is 500 m. This substantial elevation gap in the transect is due to removal of those samples with nearly blank He values. Considering this, we postulate that the ~23 Ma age should reflect the maximum onset of uplift at this location along the fault. If new data points can be produced to fill

this data gap, they may drive the models to produce a younger onset age. Therefore, we conclude that the models for the Teewinot samples are suspect and future analyses should be completed to account for the missing data along this transect. Although we cannot completely eliminate the possibility that motion on the fault is much older than previously interpreted, we exercise caution with the interpretation of the current Teewinot transect result as it stands in stark disagreement with all other Teton transects in this study and those from Brown et al. (2017). Future work will address this data gap.

REFERENCES

Anders, M. H., Geissman, J. W., Piety, L. A., and Sullivan, J. T., 1989, Parabolic distribution of eastern Snake River Plain seismicity and latest Quaternary faulting: Migratory pattern and association with the Yellowstone hotspot: Journal of Geophysical Research, v. 94, no. B2, p. 1589-1621.

Anders, M.H. and Sleep, N.H., 1992, Magmatism and extension: the thermal and mechanical effects of the Yellowstone hotspot: Journal of Geophysical Research v. 97 (B11), p. 15379-15393.

Armstrong, P.A., Ehlers, T.A., Chapman, D.S., Farley, K.A., and Kamp, P.J.J., 2003, Exhumation of the central Wasatch Mountains, Utah: 1. Patterns and timing deduced from low-temperature thermochronology data: Journal of Geophysical Research, v. 108.

Barnosky, Anthony D. 1984. The Colter formation; evidence for Miocene volcanism in Jackson Hole, Teton County, Wyoming. Earth Science Bulletin, v. 17, p. 49-97.

Barnes, J. B., Densmore, A. L., Mukul, M., Sinha, R., Jain, V., and Tandon, S. K., 2011, Interplay between faulting and base level in the development of Himalayan frontal fold topography: Journal of Geophysical Research, v. 116, no. F3.

Bergen K. J., and Shaw, J.H., 2010, Displacement profiles and displacement-length scaling relationships of thrust faults constrained by seismic-reflection data, GSA Bulletin, July/August 2010, v.122, no. 7/8, p. 1209-1219.

Brown, S. J., Thigpen, J. R., Spotila, J. A., Krugh, W. C., Tranel, L. M., & Orme, D. A. (2017). Onset timing and slip history of the Teton fault, Wyoming: A multidisciplinary reevaluation. Tectonics, 36. p. 1-24.

Braun, J., 2005, Quantitative constraints on the rate of landform evolution from low-temperature thermochronology, in Reiners, P.W. and Ehlers, T.A. eds., Low-temperature thermochronology: Techniques, Interpretations, and Applications: Mineralogical Society of America Reviews in Mineralogy and Geochemistry, v. 58, p. 351-374.

Byrd, J.O.D., Smith, R.B., and Geissman, J.W., 1994, The Teton fault, Wyoming: Topographic signature, neotectonics, and mechanisms of deformation: Journal of Geophysical Research, v. 99, no. B10, p. 20,095–20,122.

Camp, V. E., Pierce, K.L., Morgan, L.A., 2015, Yellowstone plume trigger for Basin and Range extension and coeval emplacement of the Nevada-Columbia Basin magmatic belt: Geosphere, v. 11, no. 2.

Christiansen, R.L., 2001, The Quaternary and Pliocene Yellowstone Plateau volcanic field of Wyoming, Idaho, and Montana. U. S. Geological Survey. Prof. Pap. 729-G. U. S. Geol. Survey, Denver, CO. 120 pp.

Cowie, P.A., and Scholz, C.H., 1992a, Physical explanation for the displacement length relationship of faults using a post-yield fracture-mechanics model: Journal of Structural Geology, v. 14, p. 1133–1148.

Cowie, P.A., and Scholz, C.H., 1992b, Displacement length scaling relationship for faults—Data synthesis and discussion: Journal of Structural Geology, v. 14, no. 10, p. 1149–1156.

Davarpanah, Armita and Babaie, Hassan, A., 2013, Anisotropy of fractal dimension of normal faults in northern Rocky Mountains: Implications for the kinematics of Cenozoic extension and Yellowstone hotspot's thermal expansion: Tectonophysics, v. 608, p. 530-544.

Dawers, N.H., and Anders, M.H., 1995, Displacement-length scaling and fault linkage: Journal of Structural Geology, v. 17, no. 5, p. 607–614

Dawers, N.H., Anders, M.H., and Scholz, C.H., 1993, Growth of normal faults: Displacement-length scaling: Geology, v. 21, no. 12, p. 1107–1110.

Densmore, A.L., Dawers, N.H., Gupta, S., Guidon, R., and Goldin, T., 2004, Footwall topographic development during continental extension: Journal of Geophysical Research, v. 109, F03001.

Densmore, A.L., Dawers, N.H., Gupta, S., and Guidon, R., 2005, What sets topographic relief in extensional foot-walls?: Geology, v. 33, no. 6, p. 453–456.

Ehlers, T.A., Armstrong, P.A., Chapman, D.S., 2001, Normal fault thermal regimes and the interpretation of low-temperature thermochronometers: Physics of the Earth and Planetary Interiors, v. 126, p. 179–194.

Ehlers, T.A., Farley, K.A., 2003, Apatite (U-Th)/He thermochronometry; methods and applications to problems in tectonic and surface processes: Earth and Planetary Science Letters, v. 206, no. 1–2, p. 1–14.

Ehlers, T. A., 2005, Crustal thermal processes and the interpretation of thermochronometer data, in Reiners, P. W., and Ehlers, T. A., eds., Low-Temperature Thermochronology: Techniques, Interpretations, and Applications, Volume 58: Chantilly, VA, Mineralogical Society of America, p. 315-350.

Ellis, M.A., Densmore, A.L., Anderson, R.S., 1999, Development of mountainous topography in the Basin and Ranges, USA: Basin Research, v. 11, no. 1, p. 21–41.

England, P., and Molnar, P., 1990, Surface uplift, uplift of rocks, and exhumation of rocks: Geology, v. 18, no. 12, p. 1173– 1177.

Farley, K.A., 2002, (U-Th)/He dating: Techniques, calibrations, and applications, in Portcelli, D., Ballentine, C.J., and Wieler, R., eds., Noble Gases in Geochemistry and Cosmochemistry, Volume 47: Washington, D.C., Mineralogical Society of America, p. 819–843.

Farley, K.A. and Stockli, D.F., 2002, (U-Th)/He dating of phosphates; apatite, monazite, and xenotime, in Kohn, M.J.R., John; Hughes, John M, ed., Reviews in Mineralogy and Geochemistry, Volume 48: Washington, DC, Mineralogical Society of America and Geochemical Society, p. 559-577.

Gallagher, K., 2012, Transdimensional inverse thermal history modelling for quantitative thermochronology. Journal of Geophysical Research, 117, B02408

Flowers, R.M., Ketcham, R., Shuster, D.L., Farley, K.A., 2009, Apatite (U-Th)/He thermochronology using a radiation damage accumulation and annealing model, Geochimica et Cosmochimica Acta, v. 73(8).

Gudmundsson, A., 2004, Effects of Young's modulus on fault displacement: Comptes Rendus Geoscience, v. 336, no. 1, p. 85-92.

Gudmundsson A., De Guidi G., Scudero, S. (2013) Length–displacement scaling and fault growth. Tectonophysics, v. 608: p. 1298–1309.

Hampel, A., Hetzel, R., Densmore, A.L., 2007, Postglacial slip-rate increase on the Teton normal fault, northern Basin and Range Province, caused by melting of the Yellowstone ice cap and deglaciation of the Teton Range?: Geology, v. 35, no. 12, p. 1107.

Harrison, T.M., Zeitler, P.K., 2005, Fundamentals of noble gas thermochronometry. Reviews in Mineralology and Geochememistry, v. 58, p. 123-149.

Ketcham, R.A., 2005, Forward and inverse modeling of low-temperature thermochronmetry data, in Reiners, P.W. and Ehlers, T.A. eds., Low-temperature thermochronology: Techniques, Interpretations, and Applications: Mineralogical Society of America Reviews in Mineralogy and Geochemistry, v. 58, p. 275-314, doi:10.2138/rmg.2005.58.11.

Kim, Y.S., and Sanderson, D.J., 2005, The relationship between displacement and length of faults: A review: Earth-Science Reviews, v. 68, p. 317–334.

Lageson, D.R., 1992, Possible Laramide influence on the Teton normal, western Wyoming, in Regional Geology of Eastern Idaho and Western Wyoming, edited by P.K. Link, M.A. Kuntz, and L.B. Platt: Mem. Geol. Soc. Am., v. 179, p. 183-195.

Lageson, D.R., Adams, D.C., Morgan, L.A., Pierce, K.L., and Smith, R.B., 1999, Neogene-Quaternary Tectonics and Volcanism of southern Jackson Hole, Wyoming and southeastern Idaho, in Hughes, S.S., Thackray, G.D., eds., Guidebook to the Geology of Eastern Idaho: Pocatello, Idaho Museum of Natural History, p. 115-130.

Leopold, E. B., Liu, G., Love, J. D., Love, D. W., 2007, Plio-Pleistocene climatic transition and the lifting of the Teton Range, Wyoming, Quaternary Research, 67, 1- 11.

Lippolt, H.J., Leitz, M., Wernicke, R.S., and Hagedorn, B., 1994, (U + Th) Helium dating of apatite – experience from different geochemical environments: Chemical Geology, v. 112, p. 179–191.

Love, J. D., Morgan, L. A., McIntosh, W. C., 1997, The Teewinot Formation: evidence for late Miocene basin formation in response to volcanism, faulting and uplift associated with Yellowstone hot spot?, GSA Abstracts with Programs, 29, A365.

Love, J. D., Reed, J. C., and Pierce, K. L., 2003, Creation of the Teton landscape; a geologic chronicle of Jackson hole and the Teton range: Grand Teton Natural History Association, 2nd ed.

Manighetti, I., King, G. C. P., Gaudemer, Y., Scholz, C. H., and Doubre, C., 2001, Slip accumulation and lateral propagation of active normal faults in Afar. J. Geophys. Res., 106, 13 667–13 696.

Mansfield, C. S. and Cartwright, J.A., 1996, High resolution fault displacement mapping from three-dimensional seismic data: Evidence for dip linkage during fault growth. J. Struct. Geol., 18, 249–263.

Mifflin, M. D., 1963, Geology of a part of the southern margin of the Gallatin Valley southwest Montana, Graduate Student Theses, Dissertations, & Professional Papers. 6114. M.S. thesis, 111 pp., Dept. of Geology, Montana State University, http://scholarworks.umt.edu/etd/6114

Morgan, L. A. and McIntosh, W. C., 2005, Timing and development of the Heise volcanic field, Snake River Plain, Idaho, western USA, GSA Bulletin, 117, 288-306.

Pierce, K.L., and Morgan, L.A., 2009, Is the track of the Yellowstone Hot Spot driven by a deep mantle plume? Review of volcanism, faulting, and uplift in light of new data: Journal of Volcanology and Geothermal Research, v. 188, no. 1-3, p. 1-25.

Scholz, C. H., 2002, The Mechanics of Earthquakes and Faulting, 2nd Ed. Cambridge: Cambridge University Press.

Scholz, C. H. and Cowie, P. A., 1990, Determination of total strain from faulting using slip measurements. Nature, 346, 837–838.

Scholz, C. H., Dawers, N. H., Yu, J.-Z., and Anders, M. H., 1993, Fault growth and fault scaling laws: Preliminary results. J. Geophys. Res., 98, 21 951–21 961.

Smith, R.B. and Arabasz, W.J., 1991, Seismicity of the Intermountain seismic belt, in Slemmons, D.B., Engdahl, E.R., Zoback, M.D., and Blackwell, D.D., eds., Neotectonics of North America: Geological Society of America, North America Decade Map, v.1, p.185-228.

Spotila, J. A., 2005, Applications of Low-Temperature Thermochronometry to Quantification of Recent Exhumation in Mountain Belts: Reviews in Mineralogy and Geochemistry, v. 58, no. 1, p. 449-466.

Stockli, D.F., 2005, Application of low-temperature thermochronometry to extensional tectonic settings, in Reiners, P.W., and Ehlers, T.A., eds., Low-Temperature Thermochronology: Techniques, Interpretations, & Applications: Mineralogical Society of America, Reviews in Mineralogy and Geochemistry Volume 58, p. 411–448 and references therein (e.g., Fitzgerald and Gleadow 1988; Fitzgerald et al. 1991; Howard and Foster 1996; Stockli et al. 2000).

White, B.J.P., Smith, R.B., Husen, S., Farrell, J.M., and Wong, I., 2009, Seismicity and earthquake hazard analysis of the Teton-Yellowstone region, Wyoming: Journal of Volcanology and Geothermal Research, v. 188, p. 277-296.

Zeitler, P.K., Herczeg, A.L., McDougall, I., and Honda, M., 1987, U-Th-He dating of apatite: a potential thermochronometer: Geochima et Cosmochimica Acta, v. 51, p. 2865 – 2868.

VITA

Rachel Montague Hoar

Education

B.S. Geology (2016)
James Madison University

Experience

Graduate Teaching/Research Assistant
Structure and Geodynamics Lab
Department of Earth and Environmental Sciences
University of Kentucky, 40506

Undergraduate Teaching Assistant
Physical Geology Lab and Historical Geology Lab
Department of Geology and Environmental Science
James Madison University, 22807